Received Date: 04-Dec-2013

Revised Date: 24-Apr-2014

Accepted Date: 14-May-2014

Article Type: Original Article

Combined Separation of Cu, Fe and Zn from Rock Matrices and Improved Analytical Protocols for Stable Isotope Determination

Paolo A. Sossi (1, 2)*, Galen P. Halverson (2, 3), Oliver Nebel (1) and Stephen M. Eggins (1)

(1) Research School of Earth Sciences, Australian National University, 0200 Acton, ACT, Australia
(2) School of Earth and Environmental Sciences, University of Adelaide, 5000, Adelaide, SA, Australia
(3) Department of Earth and Planetary Sciences/GEOTOP, McGill University, 3450 University Street, Montreal, QC H3A 2A7, Canada

*Corresponding author. e-mail: paolo.sossi@anu.edu.au

Isotope ratios of heavy elements vary on the 1/10000 level in high temperature materials, providing a fingerprint of the processes behind their origin. Ensuring that the measured isotope ratio is precise and accurate depends on employing an efficient chemical purification technique and optimised analytical protocols. Exploiting the disparate speciation of Cu, Fe and Zn in HCl and HNO_3, an anion-exchange chromatography procedure using AG1-X8 (200–400 mesh) and 0.4 x 7 cm Teflon columns was developed to separate them from each other and matrix elements in felsic rocks, basalts, peridotites and meteorites. It required only one pass through the resin to produce a quantitative and pure isolate, minimising preparation time, reagent consumption and total analytical blanks. Using a ThermoFinnigan Neptune Plus MC-ICP-MS, calibrator-sample bracketing with an external element spike was used to correct for mass bias. Nickel was the external element in Cu and Fe measurements, while Cu corrected Zn isotopes. These corrections were made assuming that the mass bias for the spike and analyte element was identical, and it is shown that this did not introduce any artificial bias. Measurement reproducibilities were ± 0.03‰, ± 0.04‰ and ± 0.06‰ (2*s*) for δ^{57}Fe, δ^{65}Cu and δ^{66}Zn, respectively.

Keywords: non-traditional stable isotopes, Cu, Fe, Zn isotopes, anion exchange chromatography, MC-ICP-MS, mass bias, external spike, high precision.

Received 04 Dec 13 – Accepted 14 May 14

The use of stable isotopes is becoming increasingly important in tracing geological processes. Traditionally, variations have only been resolved for light elements, (e.g.,, Li, O or C). This stems from the two principles governing the extent of mass-dependent stable isotope fractionation: the temperature and the relative mass difference ($\Delta m/m^2$) (Bigeleisen and Mayer 1947, Urey 1947). As a result, meaningful measurement of variations in isotopic abundance of heavy elements (the so-called “non-traditional” stable isotopes; such as Cr, Cu, Fe, Zn and Mo) has only been realised since the development of MC-ICP-MS, where uncertainties are an order of magnitude better than thermal ionisation mass spectrometry (TIMS) for elements with high ionisation potentials (Halliday *et al*. 1995, Rehkämper *et al*. 2001, Albarède and Beard 2004). Furthermore, as the magnitude of the fractionation decays proportional to $1/T^2$, high temperature processes demand both highly accurate and precise methodology in order to produce useful results.

The disparate geochemical properties of Cu, Fe and Zn render them applicable to different processes. The chalcophile nature of Cu lends itself to deciphering metal-sulfide equilibria in iron meteorites (Luck *et al*. 2005, Williams and Archer 2011, Bishop *et al*. 2012) and the mineralising conditions of sulfides (Ehrlich *et al*. 2004, Markl *et al*. 2006, Asael *et al*. 2007, Mathur *et al*. 2009). Copper and Zn isotope variations in carbonaceous and ordinary chondrites suggest two-three-component mixing during accretion rather than volatile loss of Zn (Luck *et al*. 2003, 2005). By contrast, Lunar mare basalts have very low Zn concentrations (≈ 3 $\mu g\ g^{-1}$) in conjunction with predominantly heavy Zn isotope values, a feature ascribed to the volatile-loss of zinc during the Moon-forming giant impact by Paniello *et al*. (2012), a common process in the nascent solar system (Herzog *et al*. 2009, Moynier *et al*. 2011). Other applications of zinc highlight its tendency to partition into fluid phases at magmatic temperatures (Toutain *et al*. 2008, Telus *et al*. 2012) and its large isotopic fractionation during biological uptake (Moynier *et al*. 2009, Kunzmann *et al*. 2013) not least of which in animals and humans (Balter *et al*. 2013, Moynier *et al*. 2013). Iron may exist in multiple valence states (0, 2+, 3+), and, coupled with its abundance as a major element, is well suited to elucidating redox processes (Williams *et al*. 2004, 2012, Rouxel *et al*. 2005, Severmann *et al*. 2008, Dauphas *et al*. 2009a, Halverson *et al*. 2011, Hibbert *et al*. 2012). As the major constituent of planetary cores, metal-silicate fractionation of iron has been investigated as a possible cause of isotopic disparity between terrestrial planets (Poitrasson *et al*. 2005, 2009, Williams *et al*. 2006, Polyakov 2009, Hin *et al*. 2012). Differences in the composition of basaltic rocks on Earth

((Schuessler *et al*. 2009, Dauphas *et al*. 2010, Nebel *et al*. 2013, Teng *et al*. 2013) and from other planets (Poitrasson *et al*. 2004b, Wang *et al*. 2012) provide clues as to their petrogenesis, source composition and oxidation state.

While the methodologies for chemical separation and measurement of Cu, Fe and Zn isotopes have been in existence for 15 years (Maréchal *et al*. 1999), they are seldom separated completely from one another and their matrix. Additionally, analytical schemes and mass bias corrections vary widely, with little consensus on best practices. We attempt to reconcile and refine these methods here, where an anion exchange chromatography procedure that quantitatively recovers Cu, Fe and Zn from a single aliquot is described. The following improvements are chronicled:

1. The reagents, resin type and dimensions have been tailored to minimise blanks and maximise separation between the analyte elements and the matrix, such that only one pass is necessary to produce a solution fit for isotopic analysis.
2. A comparison of the effect of resin characteristics (cross-linkage, particle size) and dimensions are made to further optimise the separation.
3. A quantitative basis for the use of the external substitution correction to account for mass bias (Ni for Cu and Fe; Cu for Zn) is provided, in preference to the empirical external normalisation of Maréchal *et al*. (1999).
4. The dependence of the measurement repeatability on an isotope ratio on the counting statistics for each external spike element is highlighted, and threshold values proposed.

Analyses of various reference materials that have different matrices are reported. After evaluation of the measurement reproducibilities and comparisons with previously reported values for each isotopic system, the results obtained with this methodology are shown to be both precise and accurate.

Experimental methods

Reagents, materials, standard solutions and reference materials

Double-distilled 10 mol l^{-1} HCl and 15 mol l^{-1} HNO_3 are used, diluted to lower concentrations as necessary with 18.2 MΩ cm purity Milli-Q water. All disposable components (pipette tips, columns and test tubes) were rinsed in distilled 2 mol l^{-1} HCl and Milli-Q water, while Teflon reagent bottles were refluxed with concentrated HNO_3. BioRad® PolyPrep (polypropylene) columns with a 0.8 cm diameter and 4 cm height, were loaded with ≈ 1 ml resin. To characterise the effect of column dimensions on the separation, a second set of custom-made heat-shrunk Teflon columns, with a 0.4 cm diameter and 7 cm height, resulting in a ≈ 1 ml resin bed, were used.

For isotopic determination of Cu, Fe and Zn, internationally accepted solution reference materials were used to bracket the sample data. Copper isotope ratios are given relative to NIST SRM 976 (Maréchal *et al*. 1999, Moeller *et al*. 2012), and those for Fe are quoted against IRMM-014 (Taylor *et al*. 1992), while IRMM-3702 (Ponzevera *et al*. 2006) was used as the Zn reference, re-normalised to JMC 3-0749, commonly known as JMC-Lyon (Maréchal *et al*. 1999). In all cases, conventional delta (δ) notation is used to express the ratios:

$$\delta\,{}^{n}M = \left(\frac{\left(\frac{{}^{n}M}{{}^{d}M}\right)_{\mathrm{sample}}}{\left(\frac{{}^{n}M}{{}^{d}M}\right)_{\mathrm{std}}} - 1 \right) \times 1000 \qquad (1)$$

where *n* is the numerator isotope and *d* the normalising isotope, which stays constant for all *n* isotopes of a given element, *M*. By convention, *n* > *d*.

A set of ten geological samples, which included reference materials with varying matrices, was used to test the proposed method. Copper, Fe and Zn isotopes were determined in four basalts – three from the USGS (BCR-2, BHVO-2 and BIR-1) and JB-2 from the Geological Survey of Japan (GSJ). An iron meteorite (Canyon Diablo; Smithsonian Institute), a carbonaceous chondrite (Allende CV3; Smithsonian Institute), a mantle-derived olivine (San Carlos Olivine) and an organic-rich shale (SCo-1; USGS) were also measured. A granite (JG-2; GSJ) and a peridotite (PCC-1; USGS), which contained insufficient Cu in a typical sample load to permit an analysis, were measured for Fe and Zn only.

Sample dissolution

Complete dissolution of basaltic samples (usually ≈ 25 mg) was achieved on a hot plate at 130 °C using PFA Teflon beakers, with an acid ratio of 1HCl:0.5HF:0.2HNO_3, at a concentration of 10 mol l^{-1}, 24 mol l^{-1} (48%) and 15 mol l^{-1} respectively. These were left to dissolve until there was no visible residue in the beakers, a state achieved in ≈ 48 hr. SCo-1 was also treated with H_2O_2 to oxidise the organic compounds.

Peridotites, granites, and shales were subjected to a high-pressure bomb dissolution procedure to dissolve the resistant phases present in these rocks, namely, spinel, zircon and kerogen. Samples were weighed out into 3 ml PFA Teflon vials, and a total of 1.5 ml HNO_3:HF was added at a ratio of

2:1. Five such beakers were placed in a 125 ml PTFE Teflon capsule housing with 5 ml of Milli-Q water to promote a vapour pressure in the capsule. This assembly was sealed in an iron metal bomb jacket and heated at 210 °C for 96 hr.

For both methods, 1 ml 15 mol l^{-1} HNO_3 was added periodically during subsequent evaporation to prevent the formation of insoluble fluorides. Following complete evaporation of the acid solution, the residue was dissolved in 1 ml 10 mol l^{-1} HCl, dried down again, and taken up in 1 ml 6 mol l^{-1} HCl.

Anion exchange chromatography

In our preferred procedure, BioRad AG1-X8 200–400 mesh (0.038–0.075 mm resin bead diameter) was used, a strongly basic anion exchange resin, which comprises polymerised styrene, cross-linked by divinylbenzene. The resin was cleaned by passing, successively, 3 mol l^{-1} HNO_3, Milli-Q water and 6 mol l^{-1} HCl through the columns (Table 1), where the latter step both cleans matrix elements and equilibrates the resin by converting it into chloride form.

Techniques employed to separate Cu, Fe and Zn chromatographically almost exclusively exploit their differences in speciation in a HCl medium with anion exchange resin (Strelow 1980, Maréchal *et al*. 1999, Anbar *et al*. 2000, Zhu *et al*. 2002, Luck *et al*. 2003, Archer and Vance 2004, Poitrasson and Freydier 2005, Chapman *et al*. 2006, Schoenberg and von Blanckenburg 2006, Borrok *et al*. 2007, Gioia *et al*. 2008, Yamakawa *et al*. 2009, Larner *et al*. 2011). Typically, the dissolved sample material is loaded in strong (between 6–10 mol l^{-1}) HCl, in which partition coefficients for the resin for common matrix elements, including Ca, Mg, Na and K are very low (e.g., Kraus and Nelson 1958). Copper is eluted using similar concentration (5–8 mol l^{-1} HCl, ± ascorbic acid), while Fe, in its ferric state, is removed by washing the resin with weak HCl (< 2 mol l^{-1}) or H_2O. Zinc is then eluted with weak HCl, HNO_3 or HBr.

The preferred elution scheme described here utilised a high aspect ratio column set-up (0.4 x 7 cm) to improve separation characteristics (see section 'Resin structure'). Samples were loaded onto the columns in 0.5 ml 6 mol l^{-1} HCl, where ferric chlorides in solution were visible as a yellow colouration on the resin. HCl (4 ml; mol l^{-1}) was then passed through the columns, resulting in the elution of the matrix fraction of the sample (Table 1). Addition of 7 ml of 6 mol l^{-1} HCl promoted complete elution of the Cu, together with a tail of Co. Decreasing the HCl molarity to 0.5 mol l^{-1} caused Fe (which is exclusively ferric) to desorb completely after addition of 3 ml. Zinc was then quantitatively removed from the resin with 2.5 ml 3 mol l^{-1} HNO_3. In total, 17 ml of acid were passed through the columns.

The three cuts for Cu, Fe and Zn were then evaporated to dryness, and re-dissolved in a few drops of concentrated (15.7 mol l^{-1}) HNO_3 before being evaporated. This served a dual purpose: to oxidise and expel organic species that were leached from the resin bed and could affect mass bias during measurements (Shiel *et al*. 2009) and to convert the analyte to nitrate form, nullifying the production of Cl spectral- and matrix-based polyatomic interferences. Finally, the Cu, Fe and Zn fractions were taken up in 1 ml, 5 ml and 1 ml of 2% (0.317 mol l^{-1}) HNO_3, respectively, from which dilutions to the desired concentration could then be made.

Mass spectrometry

Isotopic determinations for the three elements were performed on a ThermoFinnigan Neptune Plus MC-ICP-MS, housed at the Australian National University. Samples analysed on the ThermoFinnigan Neptune at CSIRO/University of Adelaide used an identical set up with marginally lower (80–90%) sensitivity. The mode of introduction into the mass spectrometer is critical; dry plasma and collision cell techniques are strongly susceptible to matrix effects, requiring very rigorous separation techniques as a result (Kehm *et al*. 2003, Weyer and Schwieters 2003, Archer and Vance 2004, Mason *et al*. 2004b). In this work, the ample concentration of Cu, Fe and Zn in igneous rocks permits use of the ThermoFinnigan Stable Introduction System (SIS) (Weyer and Schwieters 2003), which consists of a 50–100 μl min^{-1} low-flow glass nebuliser connected to a Scott-double pass quartz cyclonic spray chamber. The set-up facilitates greater stability and fewer nitride interferences with respect to desolvating nebulisers (Weyer and Schwieters 2003, Dauphas *et al*. 2009b). While Jet- (sample) and X-cones (skimmer) provide up to three times higher sensitivity at low and high masses, respectively, their larger apertures also increase the transmission of polyatomic molecules (such as ArO^+), with respect to the analyte element (Weyer and Schwieters 2003). As instrument sensitivity is not an issue, standard cones (sample) and H-cones (skimmer) were used in all cases, although X-cones may be considered in conjunction with medium resolution. Measurements for all elements were performed in static mode (no amplifier rotation), with the simultaneous measurement of up to seven masses (Table 2).

Copper: Separated copper fractions were diluted to 300 ng ml^{-1} solutions, and spiked with 300 ng ml^{-1} of Ni to correct for mass bias. Measurements were made in low-resolution mode, due to the absence of isobaric interferences on the Cu or Ni masses. Six masses were measured: ^{60}Ni, ^{62}N, ^{63}Cu, ^{65}Cu, ^{64}Zn and ^{66}Zn (Table 2). With the LR slits, the achievable sensitivity was typically 20 V ^{65}Cu/ppm and 2 V ^{62}Ni/ppm, yielding 7 V and 0.7 V at 300 ppb, respectively. Each cycle consisted of an idle time of 1 s and an integration over the peak centre of 4.194 s, with each analysis comprising forty cycles.

Under such conditions, the measurement repeatability was ± 0.02‰ (2*s*) on the Ni-corrected $^{65}Cu/^{63}Cu$ ratio.

Iron: Purified Fe cuts were diluted to 4 µg ml^{-1} solutions of Fe, and spiked with 8 µg ml^{-1} of Ni. ^{54}Fe, ^{56}Fe, ^{57}Fe, ^{60}Ni and ^{61}Ni were measured, and ^{53}Cr (Table 2) was monitored to correct for any ^{54}Cr interference on ^{54}Fe, although the efficient chromatographic separation of these elements meant that this correction was insignificant. Typical $^{53}Cr/^{54}Fe$ ratios were 10^{-5} to 10^{-6}, well below the threshold of 10^{-1} at which the interference correction breaks down (Dauphas *et al*. 2009b). The SIS arrangement does not appreciably reduce $^{40}Ar^{14}N^+$ and $^{40}Ar^{16,17}O^+$, on masses ^{54}Fe, ^{56}Fe and ^{57}Fe, necessitating the use of medium resolution slits to resolve between iron ions and the argide interferences (Weyer and Schwieters 2003). The ensuing mass resolution $\left(\frac{\text{[illegible]}}{\text{[illegible]}(\text{[illegible]})-\text{[illegible]}(\text{[illegible]})}\right)$ = 9000 in MR produces a plateau on ^{56}Fe, the narrowest plateau, of 200–250 ppm, given by $\frac{\text{[illegible]}-\text{[illegible]}}{\text{[illegible]}} \times 10^6$ (Poitrasson and Freydier 2005). In MR mode, the sensitivity on ^{57}Fe is approximately 0.25 V/ppm, and 0.125 V/ppm ^{61}Ni. A Ni spike was used to characterise and correct for mass bias effects. Even though the sample and skimmer cones are manufactured from Ni, they appear to have a minimal contribution to the measured $^{61}Ni/^{60}Ni$ ratios (Dauphas *et al*. 2009b, Moynier *et al*. 2007, Steele *et al*. 2011). Consistent with Poitrasson and Freydier (2005), improving the standard deviation for $^{61}Ni/^{60}Ni$ measurements by increasing the Ni signal has a marked influence on the precision of the Ni-corrected $^{57}Fe/^{54}Fe$ and $^{56}Fe/^{54}Fe$ ratios, and, accordingly, the beam size was kept at or above 1 V ^{61}Ni (see section "Measurement repeatability"). Each cycle consisted of an idle time of 1 s and an integration over the peak centre of 4.194 s, with forty-five cycles per analysis. An (in-run) measurement repeatability of ± 0.03‰ (2*s*) could be achieved on the Ni-corrected $^{57}Fe/^{54}Fe$ ratio. Given the isobaric interference of ^{58}Ni on ^{58}Fe, this mass was omitted from the measurements.

Zinc: The purified zinc column fractions were diluted to 300 ng ml^{-1} solutions and spiked with 300 ng ml^{-1} of Cu. In total, seven masses were measured: ^{63}Cu, ^{64}Zn, ^{65}Cu, ^{66}Zn, ^{67}Zn and ^{68}Zn, while ^{62}Ni was monitored to correct for the ^{64}Ni interference on ^{64}Zn (Table 2), but was proven to be insignificant ($^{62}Ni/^{64}Zn < 5 \times 10^{-4}$). As per Cu isotope determinations, the absence of isobars or polyatomic species on the Zn and Cu masses rendered the use of low resolution slits possible. Average sensitivity for ^{64}Zn was 13 V/ppm, lower than that of Cu under identical conditions, despite the higher relative abundance of ^{64}Zn (48.63 % vs. 30.83 %), consistent with the higher first ionisation energy of Zn (9.4 vs. 7.7 eV). Each cycle consisted of an idle time of 1 s and an integration over the peak centre of 4.194 s, with forty per analysis. Under such conditions, the measurement repeatability was ± 0.02‰ (2*s*) on the Ni-corrected $^{66}Zn/^{64}Zn$ ratio.

In each case, an instrumental baseline correction, which consisted of fifteen cycles with integration times of 1 s, was performed before every sample and calibrator. Following Schoenberg and von Blanckenburg (2005) and Dauphas *et al*. (2009), the concentration of the sample with respect to the calibrator, $\left(\frac{C_{\mathrm{sample}}}{C_{\mathrm{standard}}}-1\right)\times 100$, was typically matched to within 10%. However, concentration matching is less important where an external elemental spike is used to correct for mass bias.

Results and discussion

Isotopic values of reference materials

A summary of the salient characteristics of a selection commonly used Cu, Fe and Zn isotope procedures that are tailored towards rock matrices is given in online supporting information. The Cu, Fe and Zn isotope composition of the geological reference materials analysed in this work are shown in Table 3. A literature comparison of the three most commonly analysed RMs (BIR-1; BCR-2; BHVO-2) emphasising differences in the mass bias correction, instrument used and the number of analyses is presented in Figure 1.

The δ^{65}Cu values range from +0.09‰ ± 0.05 (Canyon Diablo) to -1.57‰ ± 0.09 (Allende CV3), with terrestrial basalts bracketing the NIST SRM 976 certified reference material at -0.00‰ to +0.08‰, consistent with previous studies which highlight the constancy of Cu isotopic composition in igneous rocks from Earth ((Archer and Vance 2002, Ben Othman *et al*. 2006, Li *et al*. 2009, Moeller *et al*. 2012, Liu *et al*. 2014). δ^{65}Cu values for the extra-terrestrial materials, Allende and Canyon Diablo, agree within uncertainty with published values by Luck *et al*. (2003), Moynier *et al*. (2007) and Williams and Archer (2011). The Zn mass bias correction scheme is more common, with Ni starting to become prevalent, with no obvious bias between the two (Figure 1). The JG-2 granite and PCC-1 peridotite reference materials contained insufficient copper to measure the isotope ratio using our protocol.

The iron isotopic compositions of the reference materials used in this study are well characterised (Figure 1). The prevalence of the simple CSB approach is unsurprising given the ease of separation and abundance of iron. We report the first RM data using a Ni spike for mass bias correction. While all the data overlaps, the generally larger uncertainties associated with analyses using CSB are conspicuous (Figure 1). Notably, our data for the three basaltic rocks compares favourably with values produced using the double-spike technique of Millet *et al*. (2012) (Figure 1). The importance of a careful double-spike calibration is highlighted by the analyses of Dideriksen *et al*. (2006; ‘25’, Figure 1). A 0.3‰ range in δ^{57}Fe for Canyon Diablo (Table S1 online supporting information) may be due to inhomogeneity, specifically, variable abundances of kamacite and taenite, as these two phases have significantly different isotopic compositions (Poitrasson *et al*. 2005, Williams *et al*. 2006). We also present new iron isotope compositions for two other geological reference materials, Japanese granite, JG-2 (δ^{57}Fe = +0.26‰ ± 0.02) and Cody Shale, SCo-1 (+0.04‰ ± 0.02).

Even though the newly developed IRMM-3702 certified reference material was used as the bracketing calibrator in this study, we reference our results against the JMC-Lyon reference value, as has been the custom (though both values are given in Table 3). The conversion factor between the two reference materials (Cloquet *et al*. 2008, Petit *et al*. 2008, Moeller *et al*. 2012) agrees with our own comparison ($\Delta^{66}Zn_{3702\text{-}JMC}$ = +0.30‰ ± 0.02, n = 10):

$$\delta^{66}Zn_{3702} = \delta^{66}Zn_{JMC} + 0.30 \qquad (2)$$

As revealed by previous workers (Archer and Vance 2004, Ben Othman *et al*. 2006, Chapman *et al*. 2006, Chen *et al*. 2013), the Zn isotopic composition of basaltic rocks is constant to between δ^{66}Zn = 0.2 to 0.3‰. The basalts analysed followed this norm, spanning a narrow range from 0.20‰ ± 0.03 (BIR-1) to 0.27‰ ± 0.02 (BHVO-2). Intriguingly, however, the granite JG-2 exhibited a significantly more ^{66}Zn-enriched composition, at +0.50‰ ± 0.02, suggesting a degree of Zn isotope fractionation during magmatic differentiation (Chen *et al*. 2013) as observed for Fe isotopes (Teng *et al*. 2008, Schuessler *et al*. 2009, Sossi *et al*. 2012). Additionally, the San Carlos olivine showed a marginally lighter δ^{66}Zn composition (δ^{66}Zn = 0.10‰ ± 0.03), consistent with the role of fractionating mafic phases increasing the relative abundance of heavier isotopes in the residual melt. Our value for the Allende CV3 carbonaceous chondrite, 0.22‰ ± 0.03, was indistinguishable from that of terrestrial basalts and other measurements of the meteorite (Luck *et al*. 2005, Makishima and Nakamura 2013, Table S1–3 online supporting information). Other literature data shows that the CSB + Cu correction is most widely used, with no systematic difference between instruments or methodologies, though the smaller uncertainty for samples in this study is notable. Analysis of BHVO-2 and BCR-2 using a double spike (Moeller *et al*. 2012 - ‘1’, Figure 1) are the heaviest reported for these RMs.

Crucially, column yields for all samples and over each analyte element totalled 100%, precluding any mass fractionation on the resin (see section 'Fractionation during elution').

Repeatability

Measurement repeatability: Through repeat analyses of the same sample aliquot, the uncertainty of the mean across a small number of replicate analyses are described by the 2 standard error:

$$2SE = (t_{95} \times s)/\sqrt{n} \qquad (3)$$

For a small populations ($n < 15$), a correction factor, which varies with n and the confidence limit (Student's t factor) is used to account for the small n by multiplication with the standard deviation, s.

The measurement repeatability is controlled by counting statistics, where the relative standard deviation (RSD) of an ion beam, I, is proportional to $1/\sqrt{I}$. For ratios where both isotopes have a strong signal (several volts), the dependence of the error on the signal is weak (Figure 2b, d, e, f). However, for the ^{61}Ni/^{60}Ni (and to a lesser extent, the ^{62}Ni/^{60}Ni ratio) where the beam intensities are ≈ 1 V, the effect is enhanced. The RSD on ^{57}Fe/^{54}Fe decreased from 5.5×10^{-3} at 0.25 V ^{61}Ni to 3.3×10^{-3} at 1 V ^{61}Ni, corresponding to a 50% decrease in the measurement repeatability and a 25% improvement from 0.5 V. Thus, the limiting factor is the intensity of the Ni signal and therefore the precision of the Ni mass bias correction on Cu and Fe isotopes, where ^{62}Ni and ^{61}Ni should be ≥1 V, respectively.

Following Poitrasson and Freydier (2005), the summative uncertainty on the precision of a sample analysis is given by its individual 2SE derived from repeat analysis of that sample, rather than assigning a global uncertainty to the procedure. This specificity can reveal whether a particular sample was measured less precisely, caused by issues with the sample matrix or introduction, or sudden changes in the plasma conditions.

The long-term measurement repeatability on the Milhas haematite reference material (Pyrénées, France; Williams *et al*. 2005 Sossi *et al*. 2012, Poitrasson *et al*. 2013), which was not processed chemically and analysed multiple times over the course of 12 months, was δ^{57}Fe = +0.78‰ ± 0.03 (2*s*) or ± 0.01‰ (2SE, n = 9).

Measurement reproducibility: The entire uncertainty on a sample analysis includes both components related to the mass spectrometry ('internal') and the sample processing ('external', i.e., anion exchange chromatography and wet chemistry). Assuming the external component to be negligible, the external should approach the measurement repeatability. In order to identify the sources of uncertainty for each stage of the procedure, six separate dissolutions of BHVO-2 of 10–50 mg, were processed (Table 4).

In contrast to the measurement repeatability, the measurement reproducibility of the Fe isotope determinations was better with respect to Cu and Zn. That is, the chemical processing of BHVO-2 imparts more variability on the isotopic measurement of Cu and Zn than for Fe. This may be ascribed to their relative abundances in BHVO-2, where Fe (10% *m/m*) constitutes a major fraction of the rock, while the former two are relatively impoverished (≈ 100 µg g^{-1}). Given the large dilutions (typically 500x) required to measure Fe compared with Cu and Zn (1-5x), not only are the analyte:matrix and analyte:blank ratios more favourable, but the presence of residual resin-based organics and other cryptic differences between sample and standard solutions are diminished.

In Table 4, the average, standard deviation (multiplied by 2; 2*s*) and 2SE have been calculated by pooling all analyses ('pooled'), and by considering each dissolution as a single value ('replicates'). The standard deviation describes the spread of the data rather than the uncertainty on the mean value. Equation (3), dictates that, as the number of analyses goes to infinity, the 2SE asymptotically approaches 0. However, because the 2SE is based on assumptions involving the degree of uncertainty (95% confidence in this case) and the number of replicate analyses, *n*, we also quote the standard deviation as the most fundamental measure of data precision.

To predict the expected 2SE reproducibility we employed a statistical modelling technique. In this approach, a pseudo-random number was generated about the seed mean value (here, δ^{57}Fe = 0.20‰) with the known standard deviation (± 0.03‰ 2*s*; Table 4) for twenty samples, and $2 < n < 10$. With increasing *n*, the calculated 2SE reproducibility declines proportional to 1/log from ± 0.03‰ at $n = 2$ to 0.01‰ at $n = 10$ (Figure 3a). The mean values of the BHVO-2 replicates plot within the 2SE uncertainty calculated for $n = 2$ (Figure 3b). The 2*s* reproducibility from the 1 V Ni signal (± 0.03‰, for δ^{57}Fe) is a 25% improvement over the ± 0.04‰ reported by Poitrasson and Freydier (2005) for a 0.5 V signal, mirroring the measurement repeatability (Figure 2). Thus, the uncertainties associated with this method are identical to those achieved by the double-spike technique (± 0.02‰ 2*s* δ^{56}Fe; Millet *et al*. 2012).

A measurement reproducibility (2SE) of ± 0.02‰, ± 0.02‰ and ± 0.03‰ for δ^{65}Cu, δ^{57}Fe, and δ^{66}Zn (2*s* of ± 0.03‰, ± 0.04‰ and ± 0.06‰, respectively) accurately described the uncertainty after four repetitions.

Anion exchange chromatography

Exchange capacity: Due to the finite number of exchange sites on the resin (1 meq ml^{-1} or mmol ml^{-1} for AG resins), loading excessive amounts of solute can result in premature elution of an element, a consequence of the inability of the entire budget of dissolved species to diffuse to a vacant exchange site on the resin at the imposed flow rate, causing an isotopic fractionation. Chapman *et al*. (2006) determined the breakthrough capacity for the manganese nodule NOD-P-1 on AG-MP-1 to be 20% of the theoretical exchange capacity. However, the breakthrough point is both element- and lithology-dependent. Therefore, five BHVO-2 powder masses ranging from 10–50 mg were dissolved to better constrain the resin breakthrough point for Cu, Fe and Zn for common basaltic matrices with ≈ 10% *m/m* Fe (Table 4, Figure 4).

Apparent is the substantial departure from the δ^{65}Cu mean for the ≈ 50 mg sample (Table 4), indicating a preferential loss of the heavier isotopes of Cu during the loading step, prior to Cu elution (see section 'Fractionation during elution'). The breakthrough threshold for δ^{65}Cu for basaltic samples is tentatively placed at 40 ± 10 mg, equating to 0.06 ± 0.02 meq ml^{-1}, or only 6% of the total theoretical capacity, considering that the only sorbed major element matrix species in 6 mol l^{-1} HCl is Fe^{3+} (Mg, Ca, Al have no affinity for the resin). Iron is more robust, as, even at 50 mg of dissolved BHVO-2, its isotopic composition remains unperturbed (Figure 4). However, tests on 70 mg of PCC-1 revealed Fe present in the matrix/load fraction. If the Fe breakthrough point is dependent only on the Fe content of the sample, this equates to 0.074 meq ml^{-1} for PCC-1, but higher than 0.08 meq ml^{-1} for BHVO-2. This discrepancy points to the effect of other, non-sorbing cations, such as Mg, Ca and Al. All BHVO-2 analyses of the δ^{66}Zn composition lay within 2SE uncertainty of one another at all dissolution masses (Figure 4). However, the δ^{68}Zn value for the 50 mg dissolution is non-mass dependent (Table 4), possibly a product of sample overloading. It should be noted that these tests apply only to 1 ml AG1-X8 and the protocol given in Table 1, increasing the resin volume will permit more solute to be loaded.

Resin structure: To evaluate the effect of cross-linking on elution, 1 ml of each of AG1-X4 (200–400 mesh), AG1-X8 (200–400 mesh) and AG-MP-1 (100–200 mesh) was loaded in identical columns (0.8 cm diameter, 4 cm bed height BioRad® PolyPrep columns). Independent of the resin, altering the aspect ratio of the resin bed also modifies chromatographic separation characteristics. This variable was investigated by loading custom-made heat-shrink Teflon columns, 0.4 cm in diameter with 1 ml of AG1-X8, 200–400 mesh, creating a ≈ 7 cm resin bed, representing a decrease in aspect ratio from 0.2 to 0.057.

Elution curves for Cu, Fe and Zn from BHVO-2 in AG1-X4, AG1-X8 and AG-MP-1 are shown in Figure 5. The techniques for AG-MP-1 and AG1-X4 were adapted from Maréchal *et al*. (1999) and Strelow (1980), respectively. All three strongly basic anion exchange resins were able to separate the three analyte elements from each other and the matrix. However, in detail, subtle differences between them were revealed.

The effectiveness of the separation of two elements is given by the ratio of their partition coefficients between the resin and the solvent ($D_{\mathrm{M1}}^{\mathrm{R–S}}/D_{\mathrm{M2}}^{\mathrm{R–S}}$, the separation factor). During Cu elution, a higher D_{Fe}/D_{Cu} ratios more favourable, as the intention is to retain Fe, a condition best fulfilled by the 4% and 8% cross-linked resins (Figure 6). In 8 mol l^{-1} HCl, the D_{Zn} value for AG1-X4 was 75 and resulted in premature loss of zinc (about 10%), especially with a high matrix load on the column (Figure 5c, Chapman *et al*. 2006). While D_{Zn} for AG-MP-1 in 7 mol l^{-1} HCl was indistinguishable from that of 6 mol l^{-1} HCl for AG1-X8, the lower D_{Fe}/D_{Cu} ratio of AG-MP-1, reflecting the much higher D_{Cu} (40 compared with ~16 for AG1-X4 and AG1-X8), resulted in a broad Cu elution peak, requiring 20 ml of acid (Figure 5a; Maréchal *et al*. 1999), compared with 14 for AG1-X8 and 10 for AG1-X4. Iron needs to be eluted in higher molarity HCl in AG-MP-1 to prevent the co-elution of Zn, which occurs in weak HCl (Figure 5). For these reasons, we suggest that the separation of Cu, Fe and Zn from complex matrices and Fe is best achieved using AG1-X8 (200–400 mesh).

The higher density of exchange sites on the macroporous AG-MP-1, which coat the macro- as well as micropores, should theoretically offer improved separation over solely microporous resins (AG1 series) in spite of its higher degree of cross-linkage (20–25%; (Kraus and Nelson 1958, van der Walt *et al*. 1985). In practice, the efficiency of species exchange between the mobile phase and the resin, which can be estimated by the kurtosis of the elution curve for a given element, appears to increase in the order AG-MP-1 < AG1-X8 < AG1-X4 (Figure 5). This is largely attributable to the coarser particle size of AG-MP-1 (100–200 mesh; 0.075–0.15 mm). The 200–400 mesh version would likely represent an improvement over the equivalent AG1 resins and would be the preferred choice, although it is twice as expensive.

The improvement in both the sharpness of the elution peaks and their separation is evident when comparing AG1-X8 in the high aspect ratio Teflon columns (0.4 x 7 cm) to the standard BioRad® Poly-Prep columns (0.8 x 4 cm) (Figure 5b, d). Consequently, the volume of acid required was halved from 34 to 17 ml, decreasing the blank contribution. The tailing of the elution peaks, particularly problematic for Cu, was also much reduced. These column dimensions and method were adopted as the preferred procedure.

The possibility of incomplete Cu recovery due to elution in the Fe fraction (Moeller *et al*. 2012) was observed for each of the AG resins, totalling 1–2% of the total eluted fraction. However, the reference data were in good agreement with that of previous studies (Figure 1) suggesting that this minor fraction has no impact on the isotope composition of the purified sample.
The blanks in the Cu, Fe and Zn elutions were of the order of 1 ng, 10 ng and 2 ng, respectively. Relative to the amount processed through the columns, (Cu ≈ 3000 ng; Fe ≈ 2 x 10^6 ng; Zn ≈ 3000

ng), such amounts had no effect on the measured isotopic composition. This compares with 0.15 ng of Cu, 6 ng of Fe and 0.4 ng of Zn in the same volume of double distilled 2% *v/v* HNO_3. Possible sources of increased blank contribution over the 2% nitric acid include acquisition during the evaporation step, and leaching of inorganic elemental species, particularly Zn, from the AG resins (Shiel *et al*. 2009).

Fractionation during elution: Ion exchange chromatography is predicated on the variations in speciation of an element in the solvent phase as a function of its concentration. Differential elution of an element occurs when its complexes have different selectivities for the resin. These species may also harbour different isotopic compositions. The fingerprint of isotopic fractionation resulting from incomplete yields is characterised, and potential mechanisms for this are investigated.

During sample preparation in contact with air and an oxidising acid (HNO_3), copper and iron should exist in their cupric (2^+) and ferric (3^+) states, respectively, while Zn is invariably 2^+. In aqueous solutions of changing chloride molarity, first row transition metals display similar tendencies. Namely, at low [Cl^-] activities, the metal cations are octahedrally co-ordinated in hexa-aquo ligand structure with a general form of $(M^{x+}Cl_n(H_2O)_{6-n})^{(x-n)}$, where $0 \leq n \leq 4$ (Borrok *et al*. 2007). As the activity of [Cl^-] increases, the charge on the metal-bearing complexes becomes more negative as chloride ligands predominate, increasing its selectivity for the anion resin, consistent with the monotonic increase in $D^{R\text{-}S}{}_{M}{}^{x+}$ observed experimentally (Kraus and Nelson 1958, van der Walt *et al*. 1985). The speciation of Cu, Fe and Zn in HCl is summarised by Borrok *et al*. (2007, their figs. 4, 5 and 6).

Maréchal and Albarède (2002) found a difference in δ^{65}Cu of ≈ 19‰ and ≈ 24‰ between the first and last ml quantities eluted in 7 mol l^{-1} HCl and 3 mol l^{-1} HCl respectively on AG-MP-1. Liu *et al*. (2014) found a much smaller fractionation of δ^{65}Cu ~5‰ using 8 mol l^{-1} HCl and the same resin. Zinc isotopes show reduced fractionation, ≈ 1.3‰ δ^{68}Zn (or about 0.65‰ δ^{66}Zn) in 12 mol l^{-1} HCl (Maréchal and Albarède 2002). In contrast, neither Cu nor Zn showed discernible fractionation when eluted with 0.5 mol l^{-1} HNO_3, implying that chlorocomplexes are particularly effective in inducing isotope fractionation. For iron, Anbar *et al*. (2000) record a +10‰ difference in the δ^{57}Fe values of the first and last elution cuts in 2 mol l^{-1} HCl. Roe *et al*. (2003) identified that the flow rate can affect the magnitude of the fractionation, with δ^{57}Fe values changing by ≈ 3‰ at 3 ml min^{-1}, whilst at typical analytical rates of 0.3 ml min^{-1}, this increases to ≈ 8‰.

The vector of fractionation is common to all three elements–in HCl, the initial fractions are invariably characterised by heavier isotope compositions. This may be reconciled with the relative covalent bond strength of Cl^- and H_2O ligands, as predicted by the spectrochemical series, where $H_2O > Cl^-$. The net result being that the $^{VI}Fe^{3+}$-O is shorter (≈ 2.1 Å) than the $^{IV}Fe^{3+}$-Cl bond (≈ 2.25 Å; Apted *et al*. 1985). These systematics hold for Cu^{2+}, though the Jahn-Teller distortions magnify the disparity in bond lengths around octahedrally-co-ordinated Cu, from $^{VI}Cu\text{-}O_{eq}$ = 1.95 Å and $^{VI}Cu\text{-}O_{ax}$ = 2.3 Å to $^{VI}Cu\text{-}Cl_{eq}$ = 2.3 Å and $^{VI}Cu\text{-}Cl_{ax}$ = 2.85 Å (D'Angelo *et al*. 1997), likely contributing to the larger isotopic fractionation observed for copper (Maréchal and Albarède 2002). Thus, octahedrally-co-ordinated metal hexa-aquo complexes $(M^{x+}(H_2O)_6)^x$, which, due to their positive charge, do not bind to the resin, concentrate the heavier isotopes (Hill and Schauble 2008, Black *et al*. 2011). The more strongly-sorbed tetrahedral compounds, such as $FeCl_4^-$ have lighter isotopic compositions and are eluted later (Schauble *et al*. 2001).

In our experiment, performed by eluting Fe in 0.5 mol l^{-1} using AG1-X8 (200–400 mesh) resin at typical analytical flow rates of 0.2 ml min^{-1}, a total range of 3.7‰ was observed (Figure 7) where the 1st ml had $\delta^{57}Fe$ = +1.90‰ ± 0.03 while the last fraction had $\delta^{57}Fe$ = -1.78‰ ± 0.05.

The difference between this experiment and that of Roe *et al*. (2003) is the HCl molarity. As the abundance of the $FeCl_4^-$ complex decreases with decreasing a_{Cl-}, it should constitute a smaller proportion of the extant iron complexes at 0.5 mol l^{-1} compared with 2 mol l^{-1}. Since the isotopic fractionation results from the equilibrium exchange between the sorbed $FeCl_4^-$ and the eluted $(FeCl_n[H_2O]_{6-n})^{(3-n)}$ neutral and cationic complexes, the presumed absence of the anionic species below 1 mol l^{-1} HCl should result in negligible fractionation (Anbar *et al*. 2000). However, although the magnitude of the fractionation is diminished, it is non-zero, implying the persistence of $FeCl_4^-$ to at least 0.5 mol l^{-1}.

This result highlights the requirement for 100% yield in all cases. The summative composition of BHVO-2 was $\delta^{57}Fe$ = +0.24‰ ± 0.12, in agreement with the value reported in Figure 1, indicating 100% yield. Therefore, if the Zn contents of the sample are low compared with iron, then iron should be eluted in very weak (e.g., 0.05 mol l^{-1}) HCl to expedite elution and minimise the possibility of column-based fractionation.

Mass bias correction

Mass bias, quantified by the β factor (Equation 5), is comprised of instrumental mass bias (preferential transmission of ions with higher mass/charge) and space-charge effects, which are induced by differences in matrices between sample and calibrator. Simple calibrator-sample bracketing (CSB) readily accounts for the first effect whereas external element spiking has been widely used to alleviate mass bias imposed by matrix effects. This method is based on the assumption that the element spike undergoes the same type of mass bias as the analyte element ($\beta' = \beta''$). In practice, this is not the case due to differences in mass and ionisation potential (Hirata 1996), and, as such, its application is strongly debated (Maréchal *et al*. 1999, Woodhead 2002, Archer and Vance 2004, Arnold *et al*. 2004, Poitrasson and Freydier 2005, Baxter *et al*. 2006, Peel *et al*. 2008), with two correction schemes predominating.

Empirical external normalisation (EEN): The realisation that β'/β'' is constant over short time periods gave rise to empirical external normalisation (EEN; Maréchal *et al*. 1999). The linear arrays formed by the isotope ratios of the spike and analyte in log-log space enable the β factor for the analyte to be determined empirically. The exponential and power law forms of the generalised power law, in contrast to the linear form, are consistent with respect to the ratios of ratios. In other words, considering that M_1/M_n and M_2/M_n adhere to the generalised power law, then M_2/M_1 will also exhibit a proportional mass-dependence. Importantly, Maréchal *et al*. (1999) demonstrated that mass discrimination between two elements could be best described by the exponential law (Equation 4), on the basis of its prediction that the β factor of an isotope ratio scales with its relative mass difference (Equation 5), as opposed to the mass independence as predicted by the power law. The exponential law may be written as:

$$R' = r'\left(\frac{M'_2}{M'_n}\right)^{\beta'} \qquad (4)$$

Where R' is the true ratio of (analyte) isotope pairing, r' is the measured ratio of that pairing, M'_2 is the mass of the isotope in the numerator, M'_n is the mass of the normalising isotope, and β' is its mass bias (β) factor:

$$\beta = \frac{\ln\left(\frac{R}{r}\right)}{\ln\left(\frac{M_2}{M_n}\right)} \qquad (5)$$

Taking the natural logarithm of Equation (4) for an analyte ratio (r') and a spike ratio (r''), and dividing the former by the latter results in the relationship:

$$\ln r' = \ln R' + \frac{\beta' \ln\left(\frac{M'_2}{M'_1}\right)}{\beta'' \ln\left(\frac{M''_2}{M''_1}\right)} \times (\ln r'' - \ln R'') \qquad (6)$$

In a plot of ln *r'* against ln *r''*, the slope is dependent only on the ratios of the two β factors, which are a function of the two measured ratios. Slopes in log-log space most closely resemble those estimated according to the exponential law. However, because the β factor is calculated empirically from the slope, an *a priori* assumption as to the type of law is unnecessary. The intercept is equivalent to the entire RHS of Equation (6), though it cannot be directly used to estimate the true isotope ratio, as the assumption that β'/β'' = *c* breaks down away from the ideal operating conditions of the ICP-MS. As such, the intercept is not incorporated into solving for R'_{smp} (although see Baxter *et al*. 2006).

$$R'_{smp} = r'_{smp} \left(\frac{R''}{r''_{smp}}\right)^{\frac{\beta' \ln\left(\frac{M'_2}{M'_1}\right)}{\beta'' \ln\left(\frac{M''_2}{M''_1}\right)}} \qquad (7)$$

Equation (7) quantifies the vertical deviation of the samples (represented by r''_{smp}) from the line in ln *r'* – ln *r''* space defined by the calibrators, and assuming that the samples follow the same general slope.

External substitution (ES): This correction replaces β' in Equation (4) with the β factor calculated for a second isotope pairing of the spike element, β'' (Longerich *et al*. 1987, Hirata 1996). As only the relative deviation with respect to a calibrator is required to calculate the δ value of the unknown, rather than solving for *R'* in Equation (4), we effectively solve for R'_{smp}/R'_{cal}. Since the same β'' for β' substitution is made to the bracketing calibrators too, the relative deviation of the samples from the calibrators (the δ value) is unaffected.

Equation (6) may be re-written for the analyte ratio in the calibrator and the sample:

$$\frac{\ln R'_{smp}}{\ln R'_{cal}} = \frac{\ln r'_{smp} + \beta''_{smp} \ln\left(\frac{M_2}{M_1}\right)}{\ln r'_{cal} + \beta''_{cal} \ln\left(\frac{M_2}{M_1}\right)} \qquad (8)$$

Given that β' ≠ β'' the absolute value of *R* for both calibrator and sample is systematically offset from its true value.

It is clear from Equation (8) that the assumption is not β' = β'', but rather:

$$\frac{\beta'_{smp}}{\beta'_{std}} = \frac{\beta''_{smp}}{\beta''_{std}} \tag{9}$$

Mathematically, in solving for β'$_{smp}$, this β factor may be used in conjunction with β'$_{std}$ in Equation (4) not only to yield an accurate δ value, but also to correct the sample back to its absolute ratio. In practice this is never achieved because of the disparate behaviour of the two elements in the ICP-MS.

We prefer the ES to the EEN method. Previous studies that compare the correction schemes report no systematic bias associated with either (Wombacher *et al*. 2003, Mason *et al*. 2004a, Poitrasson and Freydier 2005, Peel *et al*. 2008, Petit *et al*. 2008). Since there is no mathematical uncertainty associated with a direct substitution of β' for β'' (Equation 8), ES can be applied as effectively as the EEN correction. Due to the stability of the plasma during an analytical session, the formation of a reasonable linear relationship between (*r'*) and the spike ratio (*r''*), required for the application of the EEN, is seldom achieved, as reported in other studies (Woodhead 2002, Kehm *et al*. 2003, Archer and Vance 2004, Peel *et al*. 2008). Instead, what drift occurs typically does so as discontinuous jumps in β'/β''. The more specific ES correction, which is applied individually to each sample and calibrator, is therefore able to correct for short-term irregularities in the mass bias. In an EEN, such an anomalous point would contribute to the scatter in the slope, and we consider it counterproductive and at times inaccurate to utilise a method that is dependent on plasma instability.

Element-specific considerations

Copper: Although the majority of Cu isotope protocols use Zn as the external element (Maréchal *et al*. 1999, Archer and Vance 2004, Mason *et al*. 2004a, Chapman *et al*. 2006, Peel *et al*. 2008) we advocate the use of Ni instead. Namely, ^{62}Ni/^{60}Ni is the preferred pairing, given that ^{62}Ni is more abundant than ^{61}Ni (see section 'Measurement repeatability'). Spiking Cu solutions with Ni has been reported by Ehrlich *et al*. (2004), Larner *et al*. (2011), Li *et al*. (2009), Markl *et al*. (2006), Moeller *et al*. (2012) and Thompson *et al*. (2013). The advantages in using Ni over Zn are two-fold:

1. The first ionisation potential of Ni closely matches that of Cu (7.6 vs. 7.7 eV, respectively) whereas that of Zn is substantially higher (9.4 eV), resulting in similar β factors for Cu and Ni but not

for Zn. This is indicated by slopes of ≈ 1 in ln(^{65}Cu/^{63}Cu) vs. ln(^{62}Ni/^{60}Ni) space (Figure 8), compared with slopes ≠ 1 when plotted against ln(^{66}Zn/^{64}Zn) (Archer and Vance 2004, their figure 1).

2. The cleaner mass spectrum of Ni over Zn. The effects of Ti- and Cr-based isobars, particularly ^{48}TiO^{+} on the Zn masses are well-documented, leading to variability on the Zn-corrected δ^{65}Cu of up to several per mil (Petit *et al*. 2013, 2008), interferences that do not befall Ni. The ^{64}Zn^{1}H^{+} interference on ^{65}Cu under wet plasma conditions (Mason *et al*. 2004b), can lead to spuriously high δ^{65}Cu ratios. The degree of hydride formation monitored herein was approximately 0.001 mV per µg ml^{-1}. For 300 ng ml^{-1} Zn, this equates to 0.0001 mV**,** or a 0.02‰ increase on the δ^{65}Cu ratio for a ^{65}Cu signal of 3 V.

Of the possible polyatomic interferences on Cu masses, only those elements that are present at higher concentrations than copper (Na, Mg, Ti) present analytical difficulties, following their combination with O or Ar (Mason *et al*. 2004b, Petit *et al*. 2008, Liu *et al*. 2014). Each of these elements is theoretically quantitatively removed within the first 4 ml of the elution (Figure 5). Typical signals of ^{23}Na, ^{25}Mg and ^{49}Ti are approximately 0.02 V, 0.001 V and 0.0003 V respectively, which, given the degree of argide, oxide and hydroxide formation, have no discernible impact on the measured ^{65}Cu/^{63}Cu ratios within uncertainty (Petit *et al*. 2008).

In our procedure, Co is not perfectly separated from the Cu fraction (Figure 5; though Liu *et al*. 2014 reported complete separation using 8 mol l^{-1} HCl). Approximately half the Co budget is eluted in the matrix fraction, whereas Co and Cu co-elute in AG-MP-1 (this work; Li *et al*. 2009). In varying Cu/Co in an otherwise pure Cu solution, Li *et al*. (2009) and Liu *et al*. (2014), found no systematic difference in δ^{65}Cu between Co-free solution and for solutions with Cu/Co ratios as low as 0.1, illustrating the insensitivity of Cu isotope ratios to the presence of cobalt.

Iron: While we have shown the Ni spiking procedure (Poitrasson and Freydier 2005) to be capable of accurate and precise correction of iron isotope ratios, we also evaluate the Cu spiking, CSB and double spiking techniques.

The major drawback of Cu spiking is that the mass dispersion on the Neptune is insufficient to facilitate simultaneous collection of masses ^{53}Cr to ^{65}Cu. Instead, a peak-jumping procedure is necessary, hence increasing analysis time and inherently degrading the reproducibility of data obtained. Nevertheless, the Cu-spiking tests of Dauphas *et al*. (2009) and Schoenberg and von Blanckenburg (2005) showed no systematic offset from CSB. Indeed, our measurements using Ni spiking agree closely with the Cu-corrected values of USGS basalts by Weyer and Ionov (2007) (Figure 1).

As highlighted by Malinovsky *et al*. (2003), the accuracy of CSB measurements requires matching the analyte, acid molarity, and the purity of the matrix between sample and calibrator. The former two are readily achieved, but matrix-matching less so. In aid of this, Dauphas *et al*. (2004) enlist two passes through the resin to yield a solution of the requisite purity for analysis. As long as these safeguards are observed, precise and accurate data for each of the iron isotopes, including ^{58}Fe, can be attained by calibrator-sample bracketing alone. Evident from the data compilation (Figure 1), however, is the larger uncertainty in the measurement, even though there are no systematic offsets.

Double spiking is an attractive alternative to external element spiking, and, if the spike is added to the sample prior to column processing, can correct for any resin-induced isotopic fractionation in addition to mass bias. The $^{57\text{-}58}$Fe double spike protocol employed by Millet *et al*. (2012) has a 2*s* measurement reproducibility of ± 0.02‰ δ^{56}Fe (after 2–4 analyses); the most precise Fe isotope methodology to date (along with our own), owing, in large part, to the robustness of the mass bias correction. The only possible pitfalls are the initially laborious spike mixing and calibration.

We preferred to use the ^{57}Fe/^{54}Fe ratio because the ^{57}Fe shoulder is about 1.5 times wider (300–350 ppm) than that of ^{56}Fe, and therefore less prone to tailing effects from ArO^{+} (Weyer and Schwieters 2003), which can result in systematic shifts in the co-linearity of the mass dependence between δ^{57}Fe and δ^{56}Fe if the magnet drift (shoulder position) is not closely monitored.

Both 2% *v/v* HNO_3 (0.317 mol l^{-1}) and 0.05 mol l^{-1} HCl were used as the medium of introduction of Fe to the plasma. The rationale for using HCl over HNO_3 is that it decreased the ^{40}Ar^{14}N^{+} interference on ^{54}Fe^{+}, but since N occurs as an impurity in Ar anyway and the interferences were sufficiently resolved, there is no compelling reason to use HCl. Furthermore, 2% *v/v* HNO_3 yields better washout times and signal stability (Schoenberg and von Blanckenburg 2005).

Zinc: The Zn mass range is afflicted by numerous transition metal oxide polyatomic interferences (Mason *et al*. 2004b, Petit *et al*. 2008) that can affect the apparent mass-dependent relationship between isotope pairs. Of the matrix-based Ti-, Cr- and V-O^{+} and -OH^{+} interferences, the titanium-based isobars represent the most likely source of error (Petit *et al*. 2013). In theory, all of the Ti, Cr, and V should be removed in the first 4 ml of the matrix elution. However, up to 5–10 mV signals of ^{48}Ti^{+} may be observed in the Zn fraction ($0.002 < {}^{48}$Ti/^{64}Zn < 0.004), compared with 1 mV in double distilled 2% *v/v* HNO_3. The measured ^{48}Ti^{16}O^{+}/^{48}Ti^{+} ratio is of the order of 0.001–0.002 (0.1–0.2%) for typical wet plasma conditions (Petit *et al*. 2013). We confirmed this oxide production rate through progressive addition of Ti to a pure 300 ng ml^{-1} Zn solution at ^{48}Ti/^{64}Zn ratios of 0.0007, 0.007 and 0.07. On a ^{64}Zn signal of ≈ 2 V, the δ^{66}Zn value is decreased by 0.008‰ to 0.016‰ per 10 mV of ^{48}Ti, both within the measurement repeatability (Figure 9). As such, it is recommended that the ^{48}Ti/^{64}Zn ratio be kept below 0.005 to prevent any systematic bias in the analysis.

Even though Fe does not form any isobaric interferences on the Zn masses, its high abundance and similar behaviour on the anion exchange resin mean that it is frequently observed in purified Zn fractions at levels of up to 30 ng ml^{-1} (≈ 1 V ^{56}Fe), with corresponding Fe/Zn ratios up to 0.1. By progressively doping a pure 300 ng ml^{-1} Zn solution with 30, 300 and 3000 ng ml^{-1} of Fe, we found that it has no effect on either the δ^{66}Zn or the δ^{68}Zn ratios for Fe/Zn values up to 10, in line with Petit *et al*. (2008).

Conclusions

In this study, the effect of resin cross-linking and column dimensions on the chromatography of Cu, Fe and Zn species on strongly basic anion exchange resin was systematically investigated. Their separation could be optimised using AG1-X8 (200–400 mesh) in conjunction with a column of 0.057 width:height ratio, requiring half the total acid of conventional BioRad columns, resulting in a more time- and cost-effective separation. It is demonstrated that, although resin-induced isotopic fractionation does occur for Cu and Fe, provided the breakthrough point is not exceeded, the quantitative yields ensure that the procedure introduced no spurious results. This is substantiated by extensive comparison of reference materials analysed with this method to existing literature data, showing excellent agreement between a variety of methodologies for felsic to ultramafic matrices. Use of an external spike element to overcome mass bias effects, where the signals were sufficiently high to ensure good counting statistics, and when the correction was applied individually to each analysis of sample and their bracketing calibrators, yielded precise and accurate results. Importantly, the precision was improved owing to the efficiency of the mass bias correction and high sensitivity and stability of the ThermoFinnigan Neptune Plus MC-ICP-MS. Measurement reproducibility levels of ± 0.03‰ for δ^{57}Fe, ± 0.04 ‰ for δ^{65}Cu and ± 0.06 ‰ for δ^{65}Zn (all 2*s*) were obtained.

Acknowledgements

We are indebted to Les Kinsley and Graham Mortimer for their contributions and words of wisdom on the Neptune and clean labs, respectively. The discussions with Marcus Kunzmann about Zn isotope geochemistry are always intriguing, and similarly with Michael Ellwood about the world of low-level isotope measurements. We especially thank Julie Prytulak whose insightful comments on an earlier version of the manuscript markedly improved its clarity, tone and science. Careful and judicious evaluation of the manuscript by Frédéric Moynier and two anonymous reviewers further enhanced the paper. The professional editorial handling of Bill McDonough and Ed Williams is greatly acknowledged.

References

Albarède F. and Beard B. (2004)
Analytical methods for non-traditional isotopes. **In: Johnson C.M., Beard B.L. and Albaréde F. (eds), Geochemistry of non-traditional stable isotopes, Reviews in Mineralogy and Geochemistry. Mineralogical Society of America (Washington DC)**, 113–152.

Anbar A.D., Roe J.E., Barling J. and Nealson K.H. (2000)
Nonbiological fractionation of iron isotopes. **Science, 288**, 126–128.

Apted M.J., Waychunas G.A. and Brown G.E. (1985)
Structure and specification of iron complexes in aqueous solutions determined by X-ray absorption spectroscopy. **Geochimica et Cosmochimica Acta, 49**, 2081–2089.

Archer C. and Vance D. (2002)
Large fractionations in Fe, Cu and Zn isotopes associated with Archaean microbially-mediated sulphides. **Geochimica et Cosmochimica Acta, 66**, A26.

Archer C. and Vance D. (2004)
Mass discrimination correction in multiple-collector plasma source-mass spectrometry: An example using Cu and Zn isotopes. **Journal of Analytical Atomic Spectrometry, 19**, 656.

Arnold G.L., Weyer S. and Anbar A.D. (2004)
Fe isotope variations in natural materials measured using high mass resolution multiple collector ICP-MS. **Analytical Chemistry, 76**, 322–327.

Asael D., Matthews A., Bar-Matthews M. and Halicz L. (2007)

Copper isotope fractionation in sedimentary copper mineralization (Timna Valley, Israel). **Chemical Geology, 243**, 238–254.

Balter V., Lamboux A., Zazzo A., Télouk P., Leverrier Y., Marvel J., Moloney A.P., Monahan F.J., Schmidt O. and Albarède F. (2013)
Contrasting Cu, Fe, and Zn isotopic patterns in organs and body fluids of mice and sheep, with emphasis on cellular fractionation. **Metallomics, 5**, 1470–82.

Baxter D.C., Rodushkin I., Engström E. and Malinovsky D. (2006)
Revised exponential model for mass bias correction using an internal standard for isotope abundance ratio measurements by multi-collector inductively coupled plasma-mass spectrometry. **Journal of Analytical Atomic Spectrometry, 21**, 427–430.

Ben Othman D., Luck J.M., Bodinier J.L., Arndt N.T. and Albarède F. (2006)
Cu–Zn isotopic variations in the Earth's mantle. **Geochimica et Cosmochimica Acta, 70**, A46.

Bigalke M., Weyer S., Kobza J. and Wilcke W. (2010)
Stable Cu and Zn isotope ratios as tracers of sources and transport of Cu and Zn in contaminated soil. **Geochimica et Cosmochimica Acta, 74**, 6801–6813.

Bigeleisen J. and Mayer M.G. (1947)
Calculation of equilibrium constants for isotopic exchange reactions. **Journal of Chemical Physics, 15**, 261–267.

Bishop M.C., Moynier F., Weinstein C., Fraboulet J.-G., Wang K. and Foriel J. (2012)
The Cu isotopic composition of iron meteorites. **Meteoritics and Planetary Science, 47**, 268–276.

Black J.R., Kavner A. and Schauble E.A. (2011)
Calculation of equilibrium stable isotope partition function ratios for aqueous zinc complexes and metallic zinc. **Geochimica et Cosmochimica Acta, 75**, 769–783.

Borrok D., Wanty R., Ridley W., Wolf R., Lamothe P. and Adams M. (2007)
Separation of copper, iron, and zinc from complex aqueous solutions for isotopic measurement. **Chemical Geology, 242**, 400–414.

Chapman J.B., Mason T.F.D., Weiss D.J., Coles B.J. and Wilkinson J.J. (2006)
Chemical separation and isotopic variations of Cu and Zn from five geological reference materials. **Geostandards and Geoanalytical Research, 30**, 5–16.

Chapman J.B., Weiss D.J., Shan Y. and Lemburger M. (2009)
Iron isotope fractionation during leaching of granite and basalt by hydrochloric and oxalic acids. **Geochimica et Cosmochimica Acta, 73**, 1312–1324.

Chen H., Savage P.S., Teng F.-Z., Helz R.T. and Moynier F. (2013)
Zinc isotope fractionation during magmatic differentiation and the isotopic composition of the bulk Earth. **Earth and Planetary Science Letters, 369**, 34–42.

Cloquet C., Carignan J., Lehmann M.F. and Vanhaecke F. (2008)
Variation in the isotopic composition of zinc in the natural environment and the use of zinc isotopes in biogeosciences: A review. **Analytical and Bioanalytical Chemistry, 390**, 451–63.

Craddock P.R. and Dauphas N. (2011)
Iron isotopic compositions of geological reference materials and chondrites. **Geostandards and Geoanalytical Research, 35**, 101–123.

Craddock P.R., Warren J.M. and Dauphas N. (2013)
Abyssal peridotites reveal the near-chondritic Fe isotopic composition of the Earth. **Earth and Planetary Science Letters, 365**, 63–76.

D'Angelo P., Bottari E., Festa M.R., Nolting H.-F. and Pavel N.V. (1997)
Structural investigation of copper(II) chloride solutions using X-ray absorption spectroscopy. **Journal of Chemical Physics, 107**, 2807–2812.

Dauphas N., Craddock P.R., Asimow P.D., Bennett V.C., Nutman A.P. and Ohnenstetter D. (2009a)
Iron isotopes may reveal the redox conditions of mantle melting from Archean to Present. **Earth and Planetary Science Letters, 288**, 255–267.

Dauphas N., Janney P.E., Mendybaev R. a, Wadhwa M., Richter F.M., Davis A.M., van Zuilen M., Hines R. and Foley C.N. (2004)

Chromatographic separation and multicollection-ICP-MS analysis of iron. Investigating mass-dependent and -independent isotope effects. **Analytical Chemistry, 76**, 5855–63.

Dauphas N., Pourmand A. and Teng F.-Z. (2009b)
Routine isotopic analysis of iron by HR-MC-ICP-MS: How precise and how accurate? **Chemical Geology, 267**, 175–184.

Dauphas N., Teng F.-Z. and Arndt N.T. (2010)
Magnesium and iron isotopes in 2.7 Ga Alexo komatiites: Mantle signatures, no evidence for Soret diffusion, and identification of diffusive transport in zoned olivine. **Geochimica et Cosmochimica Acta, 74**, 3274–3291.

Dideriksen K., Baker J.A. and Stipp S.L.S. (2006)
Iron isotopes in natural carbonate minerals determined by MC-ICP-MS with a ^{58}Fe-^{54}Fe double spike. **Geochimica et Cosmochimica Acta, 70**, 118–132.

Ehrlich S., Butler I., Halicz L., Rickard D., Oldroyd A. and Matthews A. (2004)
Experimental study of the copper isotope fractionation between aqueous Cu(II) and covellite, CuS. **Chemical Geology, 209**, 259–269.

Gioia S., Weiss D., Coles B., Arnold T. and Babinski M. (2008)
Accurate and precise zinc isotope ratio measurements in urban aerosols. **Analytical Chemistry, 80**, 9776–80.

Halliday A.N., Lee D.-C., Christensen J.N., Walder A.J., Freedman P.A., Jones C.E., Hall C.M., Yi W. and Teagle D. (1995)
Recent developments in inductively coupled plasma-magnetic sector multiple collector-mass spectrometry. **International Journal of Mass Spectrometry and Ion Processes, 146/147**, 21–33.

Halverson G.P., Poitrasson F., Hoffman P.F., Nédélec A., Montel J.-M. and Kirby J. (2011)
Fe isotope and trace element geochemistry of the Neoproterozoic syn-glacial Rapitan iron formation. **Earth and Planetary Science Letters, 309**, 100–112.

Herzog G.F., Moynier F., Albarède F. and Berezhnoy A.A. (2009)

Isotopic and elemental abundances of copper and zinc in lunar samples, Zagami, Pele's hairs, and a terrestrial basalt. **Geochimica et Cosmochimica Acta, 73**, 5884–5904.

Hibbert K.E.J., Williams H.M., Kerr A.C. and Puchtel I.S. (2012)
Iron isotopes in ancient and modern komatiites: Evidence in support of an oxidised mantle from Archean to present. **Earth and Planetary Science Letters, 321–322**, 198–207.

Hill P.S. and Schauble E.A. (2008)
Modeling the effects of bond environment on equilibrium iron isotope fractionation in ferric aquo-chloro complexes. **Geochimica et Cosmochimica Acta, 72**, 1939–1958.

Hin R.C., Schmidt M.W. and Bourdon B. (2012)
Experimental evidence for the absence of iron isotope fractionation between metal and silicate liquids at 1 GPa and 1250–1300 °C and its cosmochemical consequences. **Geochimica et Cosmochimica Acta, 93**, 164–181.

Hirata T. (1996)
Lead isotopic analyses of NIST standard reference materials using multiple collector inductively coupled plasma-mass spectrometry coupled with a modified external correction method for mass discrimination effect. **Analyst, 121**, 1407.

Huang F., Zhang Z., Lundstrom C.C. and Zhi X. (2011)
Iron and magnesium isotopic compositions of peridotite xenoliths from Eastern China. **Geochimica et Cosmochimica Acta, 75**, 3318–3334.

Kehm K., Hauri E.H., Alexander C.M.O. and Carlson R.W. (2003)
High precision iron isotope measurements of meteoritic material by cold plasma ICP-MS. **Geochimica et Cosmochimica Acta, 67**, 2879–2891.

Kraus K.A. and Nelson F. (1958)
Metal separations by anion exchange. **In: Materials A.S.F.T. (ed.), Ion Exchange and Chromatography in Analytical Chemistry, ASTM Special Technical Publication, 195. ASTM International (Atlantic City)**, 27–59.

Kunzmann M., Halverson G.P., Sossi P.A., Raub T.D., Payne J.L. and Kirby J. (2013)
Zn isotope evidence for immediate resumption of primary productivity after snowball Earth. **Geology, 41**, 27–30.

Larner F., Rehkämper M., Coles B.J., Kreissig K., Weiss D.J., Sampson B., Unsworth C. and Strekopytov S. (2011)
A new separation procedure for Cu prior to stable isotope analysis by MC-ICP-MS. **Journal of Analytical Atomic Spectrometry, 26**, 1627–1632.

Li W., Jackson S., Pearson N., Alard O. and Chappell B. (2009)
The Cu isotopic signature of granites from the Lachlan Fold Belt, SE Australia. **Chemical Geology, 258**, 38–49.

Liu S.-A., Li D., Li S., Teng F.-Z., Ke S., He Y. and Lu Y. (2014)
High-precision copper and iron isotope analysis of igneous rock standards by MC-ICP-MS. **Journal of Analytical Atomic Spectrometry, 29**, 122–133.

Longerich H.P., Fryer B.J. and Strong D.F. (1987)
Determination of lead isotope ratios by inductively coupled plasma-mass spectrometry (ICP-MS). **Spectrochimica Acta Part B, 42**, 39–48.

Luck J.-M., Ben Othman D., Barrat J.A. and Albarède F. (2003)
Coupled ^{63}Cu and ^{16}O excesses in chondrites. **Geochimica et Cosmochimica Acta, 67**, 143–151.

Luck J.-M., Ben Othman D. and Albarède F. (2005)
Zn and Cu isotopic variations in chondrites and iron meteorites: Early solar nebula reservoirs and parent-body processes. **Geochimica et Cosmochimica Acta, 69**, 5351–5363.

Makishima A. and Nakamura E. (2013)
Low-blank chemistry for Zn stable isotope ratio determination using extraction chromatographic resin and double spike-multiple collector-ICP-MS. **Journal of Analytical Atomic Spectrometry, 28**, 127.

Malinovsky D., Stenberg A., Rodushkin I., Andren H., Ingri J., Öhlander B. and Baxter D.C. (2003)

Performance of high resolution MC-ICP-MS for Fe isotope ratio measurements in sedimentary geological materials. **Journal of Analytical Atomic Spectrometry, 18**, 687–695.

Maréchal C. and Albarède F. (2002)
Ion-exchange fractionation of copper and zinc isotopes. **Geochimica et Cosmochimica Acta, 66**, 1499–1509.

Maréchal C.N., Télouk P. and Albarède F. (1999)
Precise analysis of copper and zinc isotopic compositions by plasma-source mass spectrometry. **Chemical Geology, 156**, 251–273.

Markl G., Lahaye Y. and Schwinn G. (2006)
Copper isotopes as monitors of redox processes in hydrothermal mineralization. **Geochimica et Cosmochimica Acta, 70**, 4215–4228.

Mason T.F.D., Weiss D.J., Horstwood M., Parrish R.R., Russell S.S. and Coles B.J. (2004a)
High-precision Cu and Zn isotope analysis by plasma source mass spectrometry Part 2 . Correcting for mass discrimination effects. **Journal of Analytical Atomic Spectrometry, 19**, 218–226.

Mason T.F.D., Weiss D.J., Horstwood M., Parrish R.R., Russell S.S., Mullane E. and Coles B.J. (2004b)
High-precision Cu and Zn isotope analysis by plasma source mass spectrometry Part 1. Spectral interferences and their correction. **Journal of Analytical Atomic Spectrometry, 19**, 209–217.

Mathur R., Titley S., Barra F., Brantley S., Wilson M., Phillips A., Munizaga F., Maksaev V., Vervoort J. and Hart G. (2009)
Exploration potential of Cu isotope fractionation in porphyry copper deposits. **Journal of Geochemical Exploration, 102**, 1–6.

Millet M.-A., Baker J.A. and Payne C.E. (2012)
Ultra-precise stable Fe isotope measurements by high resolution multiple-collector inductively coupled plasma-mass spectrometry with a ^{57}Fe-^{58}Fe double spike. **Chemical Geology, 304–305**, 18–25.

Moeller K., Schoenberg R., Pedersen R.-B., Weiss D. and Dong S. (2012)
Calibration of the new certified reference materials ERM-AE633 and ERM-AE647 for copper and IRMM-3702 for zinc isotope amount ratio determinations. **Geostandards and Geoanalytical Research, 36**, 177–199.

Moynier F., Blichert-Toft J., Télouk P., Luck J.-M. and Albarède F. (2007)
Comparative stable isotope geochemistry of Ni, Cu, Zn, and Fe in chondrites and iron meteorites. **Geochimica et Cosmochimica Acta, 71**, 4365–4379.

Moynier F., Fujii T., Shaw A.S. and Le Borgne M. (2013)
Heterogeneous distribution of natural zinc isotopes in mice. **Metallomics, 5**, 693–699.

Moynier F., Koeberl C., Beck P., Jourdan F. and Télouk P. (2010)
Isotopic fractionation of Cu in tektites. **Geochimica et Cosmochimica Acta, 74**, 799–807.

Moynier F., Paniello R.C., Gounelle M., Albarède F., Beck P., Podosek F. and Zanda B. (2011)
Nature of volatile depletion and genetic relationships in enstatite chondrites and aubrites inferred from Zn isotopes. **Geochimica et Cosmochimica Acta, 75**, 297–307.

Moynier F., Pichat S., Pons M.-L., Fike D., Balter V. and Albarède F. (2009)
Isotopic fractionation and transport mechanisms of Zn in plants. **Chemical Geology, 267**, 125–130.

Nebel O., Arculus R.J., Sossi P.A., Jenner F.E. and Whan T.H.E. (2013)
Iron isotopic evidence for convective resurfacing of recycled arc-front mantle beneath back-arc basins. **Geophysical Research Letters, 40**, 5849–5853.

Paniello R.C., Moynier F., Beck P., Barrat J.-A., Podosek F.A. and Pichat S. (2012)
Zinc isotopes in HEDs: Clues to the formation of 4-Vesta, and the unique composition of Pecora Escarpment 82502. **Geochimica et Cosmochimica Acta, 86**, 76–87.

Peel K., Weiss D., Chapman J.B., Arnold T. and Coles B.J. (2008)
A simple combined sample-standard bracketing and inter-element correction procedure for accurate mass bias correction and precise Zn and Cu isotope ratio measurements. **Journal of Analytical Atomic Spectrometry, 23**, 103–110.

Petit J.C.J., de Jong J., Chou L. and Mattielli N. (2008)

Development of Cu and Zn isotope MC-ICP-MS measurements: Application to suspended particulate matter and sediments from the Scheldt Estuary. **Geostandards and Geoanalytical Research, 32**, 149–166.

Petit J.C.J., Taillez A. and Mattielli N. (2013)

A case study of spectral and non-spectral interferences on copper isotope measurements by multi-collector ICP-MS (wet plasma). **Geostandards and Geoanalytical Research, 37**, 319–335.

Poitrasson F., Delpech G. and Grégoire M. (2013)

On the iron isotope heterogeneity of lithospheric mantle xenoliths: Implications for mantle metasomatism, the origin of basalts and the iron isotope composition of the Earth. **Contributions to Mineralogy and Petrology, 165**, 1243–1258.

Poitrasson F. and Freydier R. (2005)

Heavy iron isotope composition of granites determined by high resolution MC-ICP-MS. **Chemical Geology, 222**, 132–147.

Poitrasson F., Halliday A.N., Lee, D.-C., Levasseur S. and Teutsch N. (2004)

Iron isotope differences between Earth, Moon, Mars and Vesta as possible records of contrasted accretion mechanisms. **Earth and Planetary Science Letters, 223**, 253–266.

Poitrasson F., Levasseur S. and Teutsch N. (2005)

Significance of iron isotope mineral fractionation in pallasites and iron meteorites for the core–mantle differentiation of terrestrial planets. **Earth and Planetary Science Letters, 234**, 151–164.

Poitrasson F., Roskosz M. and Corgne A. (2009)

No iron isotope fractionation between molten alloys and silicate melt to 2000 °C and 7.7 GPa: Experimental evidence and implications for planetary differentiation and accretion. **Earth and Planetary Science Letters, 278**, 376–385.

Polyakov V.B. (2009)

Equilibrium iron isotope fractionation at core-mantle boundary conditions. **Science, 323**, 912–914.

Ponzevera E., Quétel C.R., Berglund M., Taylor P.D.P., Evans P., Loss R.D. and Fortunato G. (2006)
Mass discrimination during MC-ICP-MS isotopic ratio measurements: Investigation by means of synthetic isotopic mixtures (IRMM-007 series) and application to the calibration of natural-like zinc materials (including IRMM-3702 and IRMM-651). **Journal of the American Society of Mass Spectrometry, 17**, 1413–1428.

Rehkämper M., Schönbächler M. and Stirling C.H. (2001)
Multiple collector ICP-MS: Introduction to instrumentation, measurement techniques and analytical capabilities. **Geostandards and Geoanalytical Research, 25**, 23–40.

Roe J.E., Anbar A.D. and Barling J. (2003)
Nonbiological fractionation of Fe isotopes: Evidence of an equilibrium isotope effect. **Chemical Geology, 195**, 69–85.

Rouxel O.J., Bekker A. and Edwards K.J. (2005)
Iron isotope constraints on the Archean and Paleoproterozoic ocean redox state. **Science, 307**, 1088–1091.

Schauble E.A., Rossman G.R. and Taylor H.P. (2001)
Theoretical estimates of equilibrium Fe-isotope fractionations from vibrational spectroscopy. **Geochimica et Cosmochimica Acta, 65**, 2487–2497.

Schoenberg R. and von Blanckenburg F. (2005)
An assessment of the accuracy of stable Fe isotope ratio measurements on samples with organic and inorganic matrices by high-resolution multicollector ICP-MS. **International Journal of Mass Spectrometry, 242**, 257–272.

Schoenberg R. and von Blanckenburg F. (2006)
Modes of planetary-scale Fe isotope fractionation. **Earth and Planetary Science Letters, 252**, 342–359.

Schuessler J.A., Schoenberg R. and Sigmarsson O. (2009)

Iron and lithium isotope systematics of the Hekla volcano, Iceland — Evidence for Fe isotope fractionation during magma differentiation. **Chemical Geology, 258**, 78–91.

Severmann S., Lyons T.W., Anbar A., McManus J. and Gordon G. (2008)
Modern iron isotope perspective on the benthic iron shuttle and the redox evolution of ancient oceans. **Geology, 36**, 487–490.

S**hiel A.E., Barling J., Orians K.J. and Weis D. (2009)**
Matrix effects on the multi-collector inductively coupled plasma-mass spectrometric analysis of high-precision cadmium and zinc isotope ratios. **Analytica Chimica Acta, 633**, 29–37.

Sonke J.E., Sivry Y., Viers J., Freydier R., Dejonghe L., André L., Aggarwal J.K., Fontan F. and Dupré B. (2008)
Historical variations in the isotopic composition of atmospheric zinc deposition from a zinc smelter. **Chemical Geology, 252**, 145–157.

Sossi P.A., Foden J.D. and Halverson G.P. (2012)
Redox-controlled iron isotope fractionation during magmatic differentiation: an example from the Red Hill intrusion, S. Tasmania. **Contributions to Mineralogy and Petrology, 164**, 757–772.

Steele R.C.J., Elliott T., Coath C.D. and Regelous M. (2011)
Confirmation of mass-independent Ni isotopic variability in iron meteorites. **Geochimica et Cosmochimica Acta, 75**, 7906–7925.

Strelow F.W.E. (1980)
Improved separation of iron from copper and other elements by anion-exchange chromatography on a 4% cross-linked resin with high concentrations of hydrochloric acid. **Talanta, 27**, 727–732.

Taylor P.D.P., Maeck R. and De Bièvre P. (1992)
Determination of the absolute isotopic composition and atomic weight of a reference sample of natural iron. **International Journal of Mass Spectrometry and Ion Processes, 121**, 111–125.

Telus M., Dauphas N., Moynier F., Tissot F.L.H., Teng F.-Z., Nabelek P.I., Craddock P.R. and Groat L.A. (2012)

Iron, zinc, magnesium and uranium isotopic fractionation during continental crust differentiation: The tale from migmatites, granitoids, and pegmatites. **Geochimica et Cosmochimica Acta, 97**, 247–265.

Teng F.-Z., Dauphas N. and Helz R.T. (2008)
Iron isotope fractionation during magmatic differentiation in Kilauea Iki lava lake. **Science, 320**, 1620–2.

Teng F.-Z., Dauphas N., Huang S. and Marty B. (2013)
Iron isotopic systematics of oceanic basalts. **Geochimica et Cosmochimica Acta, 107**, 12–26.

Thompson C.M., Ellwood M.J. and Wille M. (2013)
A solvent extraction technique for the isotopic measurement of dissolved copper in seawater. **Analytica Chimica Acta, 775**, 106–13.

Toutain J.-P., Sonke J., Munoz M., Nonell A., Polvé M., Viers J., Freydier R., Sortino F., Joron J.-L. and Sumarti S. (2008)
Evidence for Zn isotopic fractionation at Merapi volcano. **Chemical Geology, 253**, 74–82.

Urey H.C. (1947)
The thermodynamic properties of isotopic substances. **Journal of the Chemical Society,** 562–581.

Van der Walt T.N., Strelow F.W.E. and Verheij R. (1985)
The Influence of crosslinkage on the distribution coefficients and anion exchange behaviour of some elements in hydrochloric acid. **Solvent Extr. Ion Exch. 3**, 723–740.

Viers J., Oliva P., Nonell A., Gélabert A., Sonke J.E., Freydier R., Gainville R. and Dupré B. (2007)
Evidence of Zn isotopic fractionation in a soil–plant system of a pristine tropical watershed (Nsimi, Cameroon). **Chemical Geology, 239**, 124–137.

Wang K., Moynier F., Dauphas N., Barrat J.-A., Craddock P. and Sio C.K. (2012)
Iron isotope fractionation in planetary crusts. **Geochimica et Cosmochimica Acta, 89**, 31–45.

Weinstein C., Moynier F., Wang K., Paniello R., Foriel J., Catalano J. and Pichat S. (2011)

Isotopic fractionation of Cu in plants. **Chemical Geology, 286**, 266–271.

Weyer S., Anbar A.D., Brey G.P., Muenker C., Mezger K. and Woodland A.B. (2005)
Iron isotope fractionation during planetary differentiation. **Earth and Planetary Science Letters, 240**, 251–264.

Weyer S. and Ionov D.A. (2007)
Partial melting and melt percolation in the mantle: The message from Fe isotopes. **Earth and Planetary Science Letters, 259**, 119–133.

Weyer S. and Schwieters J.B. (2003)
High precision Fe isotope measurements with high mass resolution MC-ICP-MS. **International Journal of Mass Spectrometry, 226**, 355–368.

Williams H.M. and Archer C. (2011)
Copper stable isotopes as tracers of metal–sulphide segregation and fractional crystallisation processes on iron meteorite parent bodies. **Geochimica et Cosmochimica Acta, 75**, 3166–3178.

Williams H.M., Markowski A., Quitté G., Halliday A.N., Teutsch N. and Levasseur S. (2006)
Fe isotope fractionation in iron meteorites: New insights into metal-sulphide segregation and planetary accretion. **Earth and Planetary Science Letters, 250**, 486–500.

Williams H.M., McCammon C.A., Peslier A.H., Halliday A.N., Teutsch N., Levasseur S. and Burg J-P. (2004)
Iron isotope fractionation and the oxygen fugacity of the mantle. **Science, 304**, 1656–9.

Williams H.M., Peslier A.H., McCammon C., Halliday A.N., Levasseur S., Teutsch N. and Burg J-P. (2005)
Systematic iron isotope variations in mantle rocks and minerals: The effects of partial melting and oxygen fugacity. **Earth and Planetary Science Letters, 235**, 435–452.

Williams H.M., Wood B.J., Wade J., Frost D.J. and Tuff J. (2012)
Isotopic evidence for internal oxidation of the Earth's mantle during accretion. **Earth and Planetary Science Letters, 321–322**, 54–63.

Wombacher F., Rehkämper M., Mezger K. and Münker C. (2003)
Stable isotope compositions of cadmium in geological materials and meteorites determined by multiple-collector ICP-MS. **Geochimica et Cosmochimica Acta, 67**, 4639–4654.

Woodhead J. (2002)
A simple method for obtaining highly accurate Pb isotope data by MC-ICP-MS. **Journal of Analytical Atomic Spectrometry, 17**, 1381–1385.

Yamakawa A., Yamashita K., Makishima A. and Nakamura E. (2009)
Chemical separation and mass spectrometry of Cr, Fe, Ni, Zn and Cu in terrestrial and extraterrestrial materials using thermal ionization mass spectrometry. A**nalytical Chemistry, 81**, 9787–94.

Zhao X., Zhang H., Zhu X., Tang S. and Yan B. (2012)
Iron isotope evidence for multistage melt–peridotite interactions in the lithospheric mantle of eastern China. **Chemical Geology, 292–293**, 127–139.

Zhu X.K., Guo Y., Williams R.J.P., O'Nions R.K., Matthews A., Belshaw N.S., Canters G.W., de Waal E.C., Weser U., Burgess B.K. and Salvato B. (2002)
Mass fractionation processes of transition metal isotopes. **Earth and Planetary Science Letters, 200**, 47–62.

Supporting information

The following supporting information is available online:

Tables S1–3. Cu, Fe and Zn data for reference materials measured in this study and from the literature.

This material is available as part of the online article from:
http://onlinelibrary.wiley.com/doi/10.1111/j.1751-908X.2014.00298.x/abstract
(This link will take you to the article abstract).

Figure Captions

Figure 1. Compilation of δ^{65}Cu, δ^{57}Fe and δ^{66}Zn data for the three most commonly analysed RMs (BIR-1, BHVO-2 and BCR-2). Also given are the weighted averages (black line) and their associated 1 standard deviation (grey envelope). Numbers correspond to data sources (full list in online supporting information): 1. Moeller *et al*. (2012) 2. Archer and Vance (2002) 3. Bigalke *et al*. (2010) 4. Moynier *et al*. (2010) 5. Li *et al*. (2009) 8. Liu *et al*. (2014) 9. Weinstein *et al*. (2011) 10. Wang *et al*. (2012) 11. Craddock *et al*. (2013) 12. Dauphas *et al*. (2009a) 16. Williams *et al*. (2005) 17. Weyer *et al*. (2005) 18.Schuessler *et al*. (2009) 19. Poitrasson *et al*. (2005, 2004a) 20. Schoenberg and von Blanckenburg (2006) 22. Hibbert *et al*. (2012) 23. Huang *et al*. (2011) 24. Zhao *et al*. (2012) 25. Dideriksen *et al*. (2006) 26. Chapman *et al*. (2009) 27. Craddock and Dauphas (2011) 28. Millet *et al*. (2012) 30. Archer and Vance (2004) 31. Chapman *et al*. (2006) 32. Cloquet *et al*. (2008) 33. Viers *et al*. (2007) 34. Toutain *et al*. (2008) 35. Sonke *et al*. (2008) 36. Herzog *et al*. (2009) 37. Bigalke *et al*. (2010) 38. Moynier *et al*. (2011) 41. Chen *et al*. (2013).

Figure 2. Illustration of how the measurement repeatability on the external element spike corrected Cu, Fe and Zn ratios vary with (a) ^{62}Ni intensity (b) ^{65}Cu intensity (c) ^{61}Ni intensity (d) ^{57}Fe intensity (e) ^{65}Cu intensity and (f) ^{64}Zn intensity. Note the log scale on the abscissa on parts (a) and (b).

Figure 3: The measurement reproducibility of the δ^{57}Fe value as modelled by pseudo-random number generation. (a) The change in the standard deviation and 2SE value as a function of repetitions (b) the mean value of these populations compared with the seed and the actual measurements.

Figure 4. The variation in isotopic composition with the amount of sample passed through the columns. All samples fell within uncertainty of each other up to ≈ 50 mg, where δ^{65}Cu was strongly negative (-2.03‰, off scale).

Figure 5. Elution curves for Cu, Fe and Zn from BHVO-2 in (a) AG-MP-1 (100–200 mesh), (b) AG1-X8 (200–400 mesh), (c) AG1-X4 (200–400 mesh) and (d) AG1-X8 (200–400 mesh) in 0.4:7 cm aspect ratio columns. X-scale is identical for each experiment.

Figure 6. The separation factor for Fe and Cu against the partition coefficient of Zn for the resin are compared for AG-MP-1; AG1-X4 and AG1-X8 in 7, 8 and 6 mol l^{-1} HCl loading solution, respectively. Desired conditions occur at high D_{Fe}/D_{Cu} and high D_{Zn}, which was optimised in AG1-X8 resin.

Figure 7. Iron isotope fractionation associated with its progressive elution from the resin, taken at 1 ml intervals. Superimposed on this is the curve showing the relative fraction of iron in each cut.

Figure 8. The linear correlation between isotopes of copper (analyte) and nickel (external spike) in low resolution mode over 1.5 years (16/11/2011 to 4/5/2013) illustrating that the slope conforms to a value of 1, indicative of similar β factors.

Figure 9: The effect of the $^{48}Ti^{16}O^+$ interference on the measured $^{66}Zn/^{64}Zn$ ratios as a function of $^{48}Ti/^{64}Zn$ ratio. The different series correspond to different extents of oxide formation, which, at typical conditions, was around 0.2% of the ^{48}Ti signal, shown by the data (black diamonds). The threshold of analytical uncertainty occurs at ± 0.03‰ (2SE).

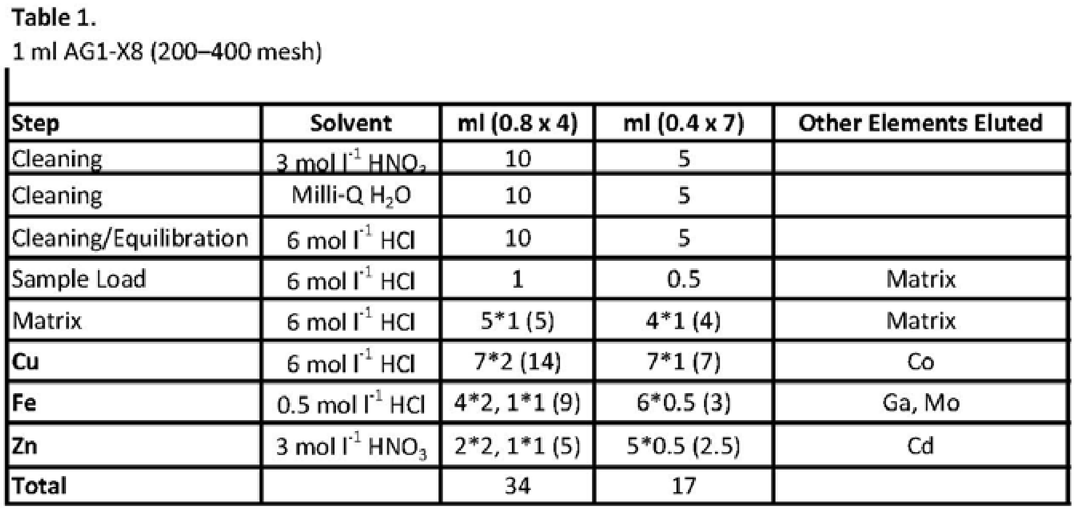

Table 1.
1 ml AG1-X8 (200–400 mesh)

Step	Solvent	ml (0.8 x 4)	ml (0.4 x 7)	Other Elements Eluted
Cleaning	3 mol l^{-1} HNO_3	10	5	
Cleaning	Milli-Q H_2O	10	5	
Cleaning/Equilibration	6 mol l^{-1} HCl	10	5	
Sample Load	6 mol l^{-1} HCl	1	0.5	Matrix
Matrix	6 mol l^{-1} HCl	5*1 (5)	4*1 (4)	Matrix
Cu	6 mol l^{-1} HCl	7*2 (14)	7*1 (7)	Co
Fe	0.5 mol l^{-1} HCl	4*2, 1*1 (9)	6*0.5 (3)	Ga, Mo
Zn	3 mol l^{-1} HNO_3	2*2, 1*1 (5)	5*0.5 (2.5)	Cd
Total		34	17	

Table 2.
Cup configurations employed on the ThermoFinnigan Neptune Plus instrument

Cup	L4	L3	L2	L1	C	H1	H2	H3	H4
Cu	^{60}Ni		^{62}Ni	^{63}Cu	^{64}Zn	^{65}Cu	^{66}Zn		
Fe	^{53}Cr		^{54}Fe	^{56}Fe	^{57}Fe		^{60}Ni		^{61}Ni
Zn		^{62}Ni	^{63}Cu	^{64}Zn	^{65}Cu	^{66}Zn	^{67}Zn	^{68}Zn	

Table 3.
Summary of the isotopic composition (δ^{65}Cu, δ^{57}Fe, δ^{66}Zn) of reference materials obtained in this work

	$\delta^{65}Cu_{976}$	2*s*	2SE	n		$\delta^{57}Fe_{014}$	2*s*	2SE	n		$\delta^{66}Zn_{3702}$	$\delta^{66}Zn_{Lyon}$	2*s*	2SE	n
BCR-2	0.08	0.05	0.04	2		0.14	0.02	0.02	2		-0.05	0.25	0.01	0.01	3
BHVO-2	0.01	0.04	0.01	12		0.20	0.03	0.01	14		-0.03	0.27	0.06	0.02	18
JB-2	0.06	0.08	0.06	2		0.10	0.03	0.02	3		-0.08	0.22	0.07	0.06	2
JG-2	N/A										0.20	0.50	0.02	0.02	2
San Carlos #1	0.03	0.02	0.02	2		0.02	0.05	0.04	2		-0.18	0.12	0.01	0.01	2
San Carlos #2	0.01	0.03	0.03	2							-0.23	0.07	0.03	0.02	3
BIR-1	0.00	0.03	0.02	2		0.09	0.01	0.01	2		-0.10	0.20	0.04	0.03	2
Allende CV3						0.01	0.05	0.04	3						
Canyon Diablo						0.00	0.07	0.05	3						
Allende CV3 B	-1.57	0.13	0.09	3		0.01	0.08	0.06	3		-0.08	0.22	0.03	0.03	2
Canyon Diablo	0.09	0.06	0.05	2		0.04	0.03	0.02	3		1.82	2.12	0.05	0.04	2
JG 2 B	N/A					0.26	0.02	0.02	3		0.21	0.51	0.04	0.03	2
PCC-1 B	N/A					0.07	0.03	0.02	3		-0.09	0.21	0.05	0.04	3
SCo-1 B	-0.16	0.01	0.01	2		0.04	0.02	0.02	3		-0.10	0.20	0.01	0.01	2
HEM	N/A					0.78	0.03	0.01	9		N/A				

B = high pressure Parr bomb dissolution.

Table 4.
The Cu, Fe and Zn isotope compositions of replicates of varying masses of BHVO-2

Replicate	Mass (g)	n	δ^{56}Fe	2*s*	2SE		δ^{57}Fe	2*s*	2SE		n	δ^{65}Cu	2*s*	2SE		n	δ^{66}Zn	2*s*	2SE		δ^{68}Zn	2*s*	2SE
0	0.02466	2	0.13	0.03	0.02		0.19	0.04	0.03		2	0.03	0.00	0.02		3	0.24	0.03	0.02		0.48	0.06	0.05
1	0.01806	2	0.13	0.00	0.00		0.19	0.00	0.00		3	0.04	0.04	0.03		3	0.28	0.06	0.04		0.54	0.12	0.08
2	0.01943	2	0.13	0.03	0.02		0.19	0.04	0.03		3	0.01	0.04	0.03		3	0.27	0.02	0.01		0.52	0.04	0.03
3	0.02908	2	0.13	0.02	0.02		0.19	0.01	0.01		2	0.01	0.04	0.03		3	0.31	0.06	0.04		0.62	0.12	0.08
4	0.05288	2	0.13	0.02	0.02		0.21	0.05	0.04		2	*-2.03*	*0.12*	*0.08*		3	0.26	0.04	0.03		*0.60*	*0.08*	*0.06*
5	0.01158	2	0.12	0.03	0.02		0.21	0.04	0.03		2	-0.01	0.04	0.03		3	0.26	0.06	0.04		0.50	0.10	0.07
Adelaide		2	0.13	0.03	0.02		0.20	0.04	0.03														
Average (replicates)		**7**	**0.13**	**0.01**	**0.01**		**0.20**	**0.01**	**0.01**		**5**	**0.02**	**0.04**	**0.02**		**6**	**0.27**	**0.05**	**0.02**		**0.53**	**0.11**	**0.04**
Average (pooled)		**14**	**0.13**	**0.02**	**0.01**		**0.20**	**0.03**	**0.01**		**12**	**0.02**	**0.04**	**0.01**		**18**	**0.27**	**0.06**	**0.01**		**0.53**	**0.13**	**0.03**

Adelaide = BHVO-2 processed and run on the Neptune instrument at the CSIRO/University of Adelaide.

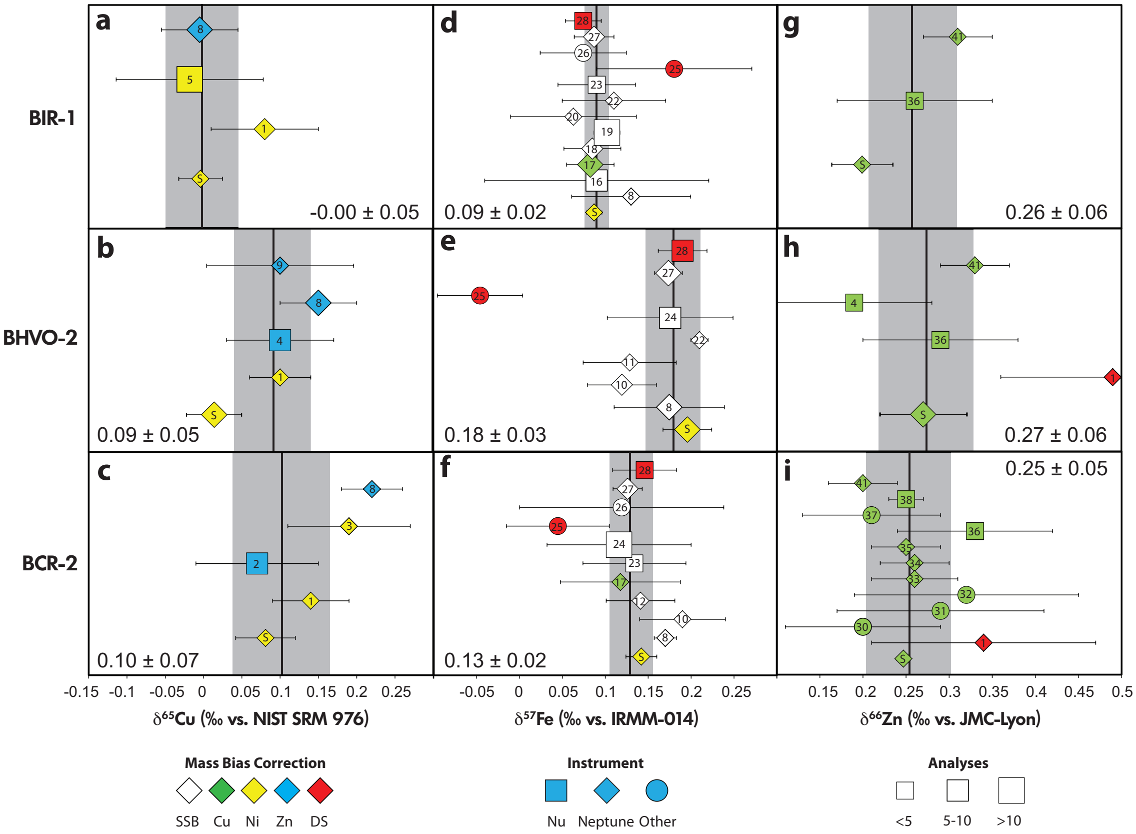
BIR-1
BHVO-2
BCR-2
a
-0.00 ± 0.05
b
0.09 ± 0.05
c
0.10 ± 0.07
d
0.09 ± 0.02
e
0.18 ± 0.03
f
0.13 ± 0.02
g
0.26 ± 0.06
h
0.27 ± 0.06
i
0.25 ± 0.05
-0.15 -0.1 -0.05 0 0.05 0.1 0.15 0.2 0.25
δ65Cu (‰ vs. NIST SRM 976)
-0.05 0 0.05 0.1 0.15 0.2 0.25
δ57Fe (‰ vs. IRMM-014)
0.15 0.2 0.25 0.3 0.35 0.4 0.45 0.5
δ66Zn (‰ vs. JMC-Lyon)
Mass Bias Correction
SSB Cu Ni Zn DS
Instrument
Nu Neptune Other
Analyses
<5 5-10 >10

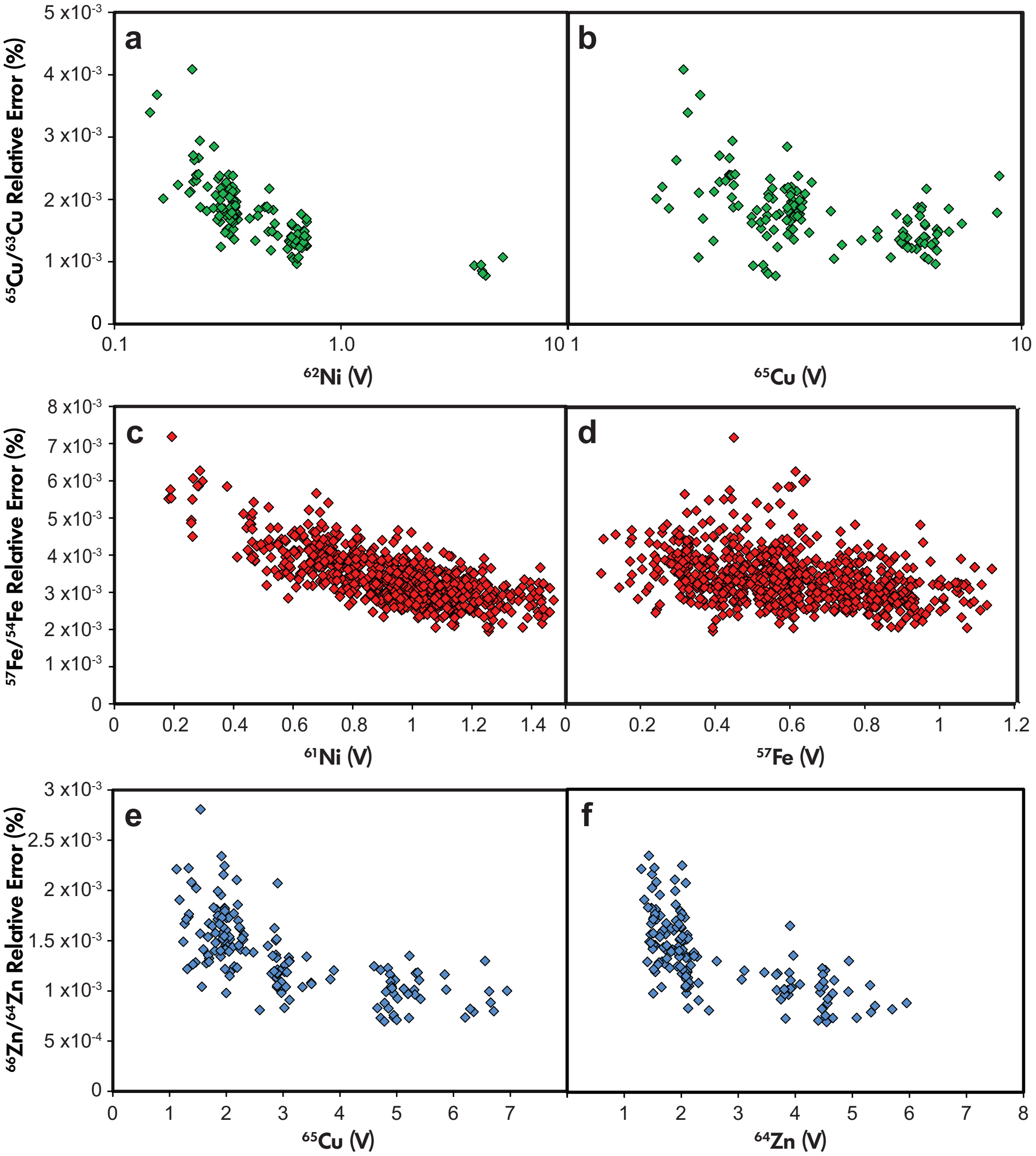
a
b
^{65}Cu/^{63}Cu Relative Error (%)
5 x10^{-3}
4 x10^{-3}
3 x10^{-3}
2 x10^{-3}
1 x10^{-3}
0
0.1
1.0
10
1
10
^{62}Ni (V)
^{65}Cu (V)
c
d
^{57}Fe/^{54}Fe Relative Error (%)
8 x10^{-3}
7 x10^{-3}
6 x10^{-3}
5 x10^{-3}
4 x10^{-3}
3 x10^{-3}
2 x10^{-3}
1 x10^{-3}
0
0 0.2 0.4 0.6 0.8 1 1.2 1.4
0 0.2 0.4 0.6 0.8 1 1.2
^{61}Ni (V)
^{57}Fe (V)
e
f
^{66}Zn/^{64}Zn Relative Error (%)
3 x10^{-3}
2.5 x10^{-3}
2 x10^{-3}
1.5 x10^{-3}
1 x10^{-3}
5 x10^{-4}
0
0 1 2 3 4 5 6 7
1 2 3 4 5 6 7 8
^{65}Cu (V)
^{64}Zn (V)

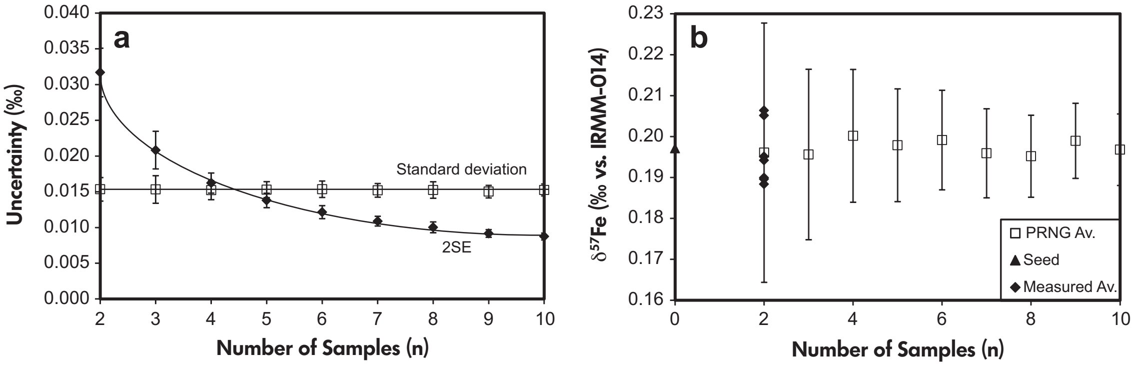
a
Uncertainty (‰)
0.040
0.035
0.030
0.025
0.020
0.015
0.010
0.005
0.000
Standard deviation
2SE
2
3
4
5
6
7
8
9
10
Number of Samples (n)
b
δ57Fe (‰ vs. IRMM-014)
0.23
0.22
0.21
0.20
0.19
0.18
0.17
0.16
0
2
4
6
8
10
Number of Samples (n)
PRNG Av.
Seed
Measured Av.

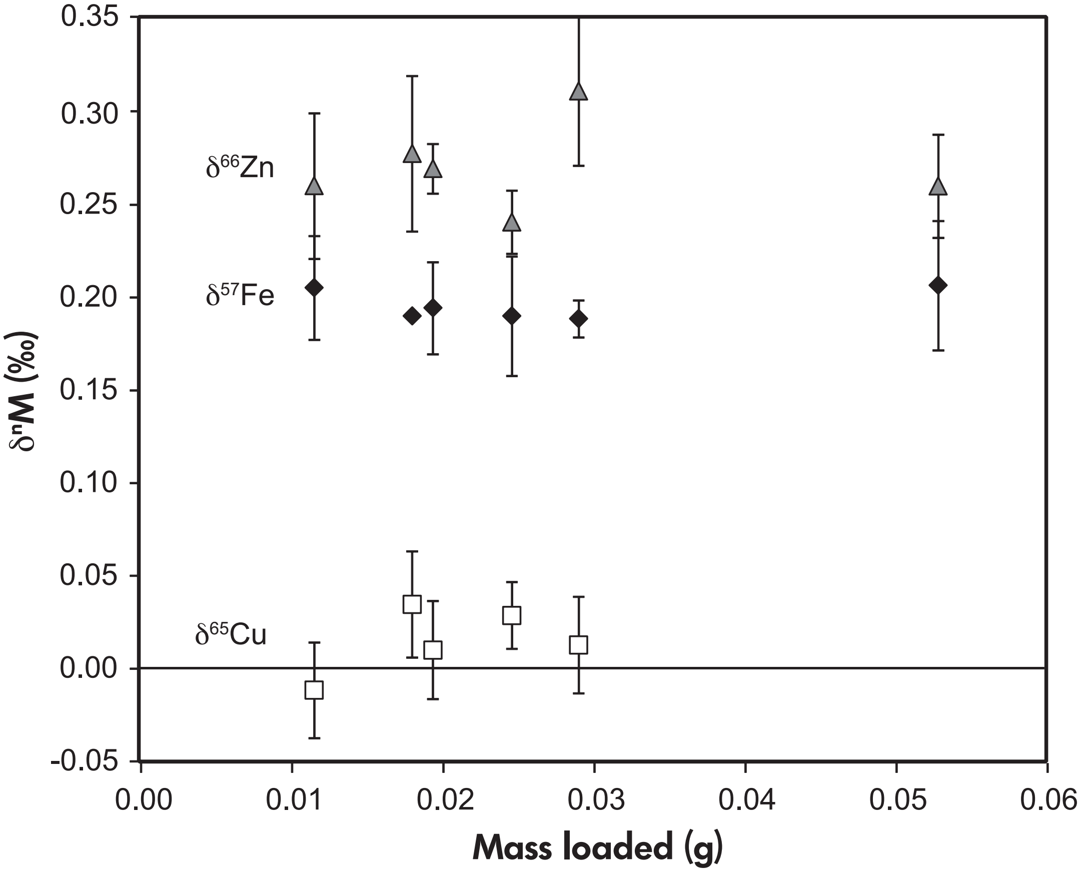
δ66Zn
δ57Fe
δ65Cu
δnM (‰)
0.35
0.30
0.25
0.20
0.15
0.10
0.05
0.00
-0.05
0.00
0.01
0.02
0.03
0.04
0.05
0.06
Mass loaded (g)

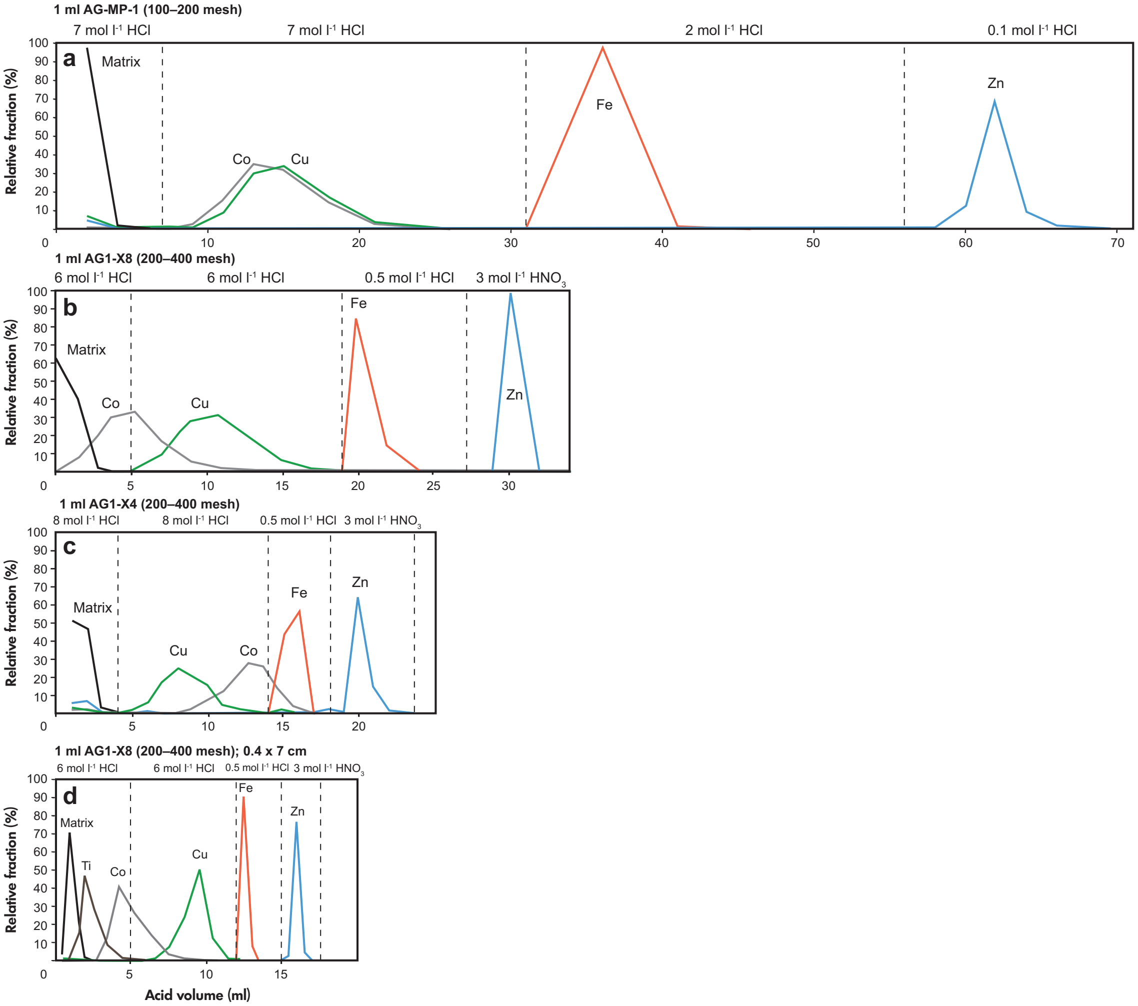
1 ml AG-MP-1 (100–200 mesh)
7 mol l-1 HCl
7 mol l-1 HCl
2 mol l-1 HCl
0.1 mol l-1 HCl
a
Matrix
Co
Cu
Fe
Zn
Relative fraction (%)
0
10
20
30
40
50
60
70
80
90
100
0
10
20
30
40
50
60
70
1 ml AG1-X8 (200–400 mesh)
6 mol l-1 HCl
6 mol l-1 HCl
0.5 mol l-1 HCl
3 mol l-1 HNO3
b
Matrix
Co
Cu
Fe
Zn
Relative fraction (%)
0
5
10
15
20
25
30
1 ml AG1-X4 (200–400 mesh)
8 mol l-1 HCl
8 mol l-1 HCl
0.5 mol l-1 HCl
3 mol l-1 HNO3
c
Matrix
Cu
Co
Fe
Zn
Relative fraction (%)
0
5
10
15
20
1 ml AG1-X8 (200–400 mesh); 0.4 x 7 cm
6 mol l-1 HCl
6 mol l-1 HCl
0.5 mol l-1 HCl
3 mol l-1 HNO3
d
Matrix
Ti
Co
Cu
Fe
Zn
Relative fraction (%)
0
5
10
15
Acid volume (ml)

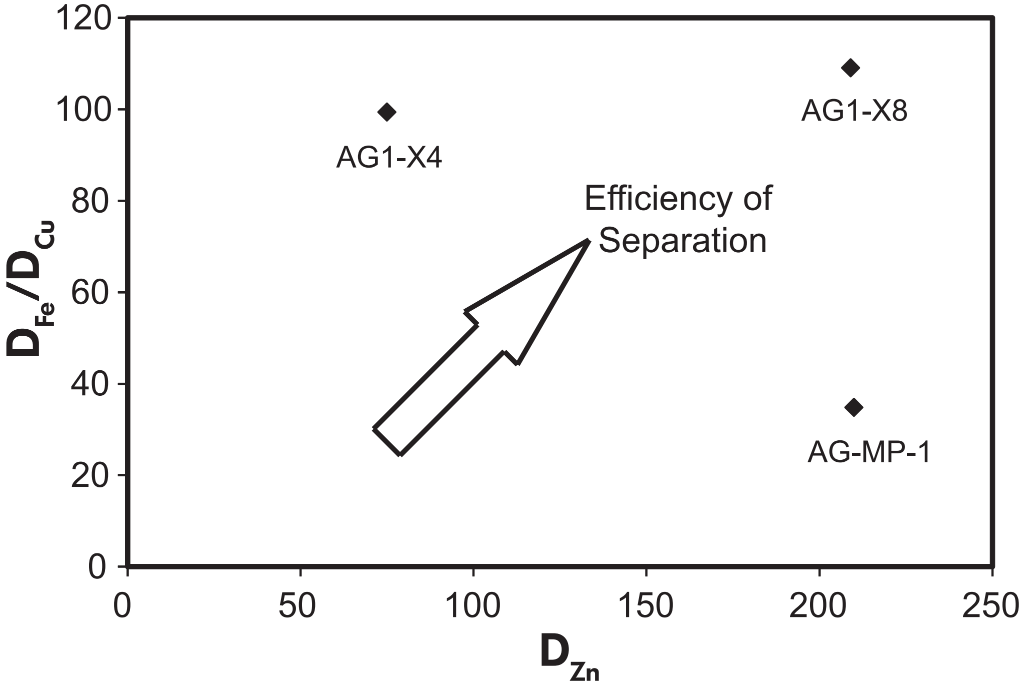
120
100
80
60
40
20
0
0
50
100
150
200
250
D_{Fe}/D_{Cu}
D_{Zn}
AG1-X4
AG1-X8
AG-MP-1
Efficiency of Separation

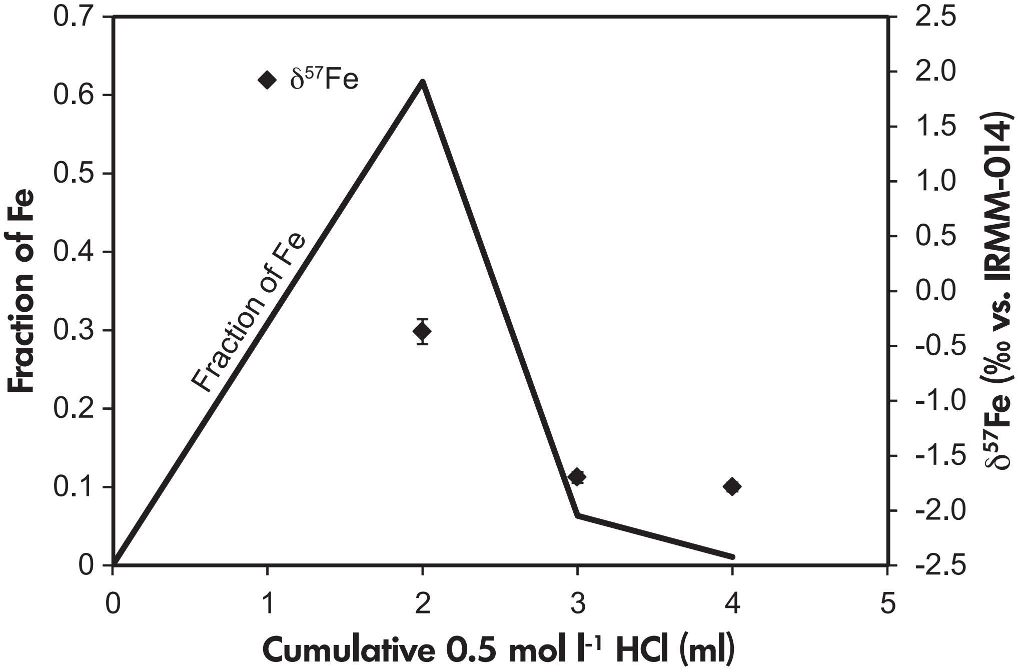
0.7
0.6
0.5
0.4
0.3
0.2
0.1
0
2.5
2.0
1.5
1.0
0.5
0.0
-0.5
-1.0
-1.5
-2.0
-2.5
0
1
2
3
4
5
Fraction of Fe
δ^{57}Fe (‰ vs. IRMM-014)
Cumulative 0.5 mol l^{-1} HCl (ml)
◆ δ^{57}Fe
Fraction of Fe

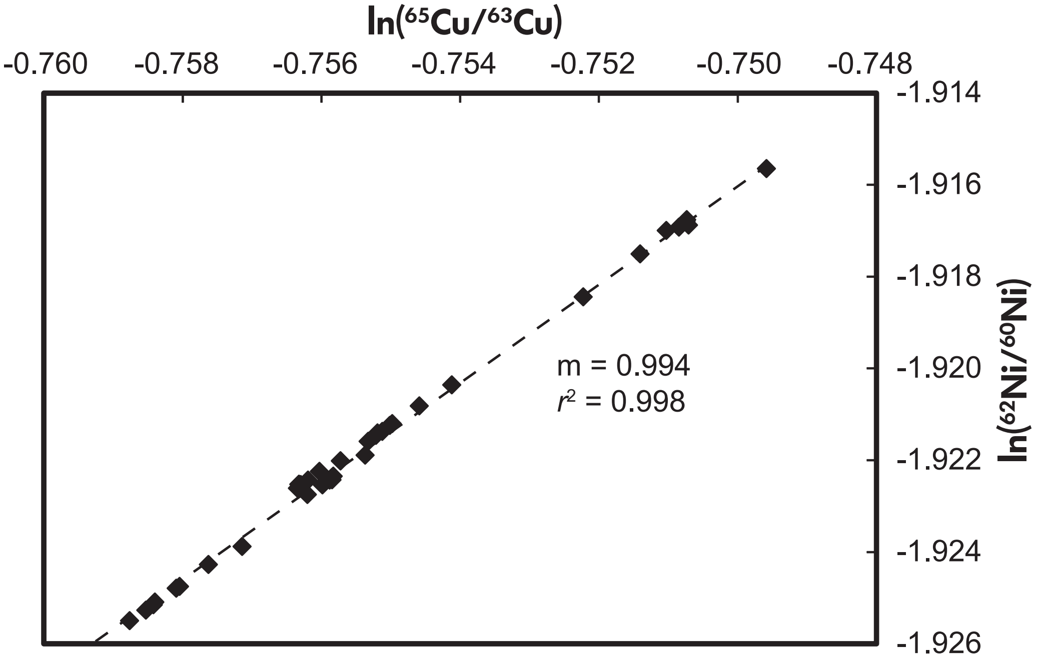
ln(⁶⁵Cu/⁶³Cu)
-0.760
-0.758
-0.756
-0.754
-0.752
-0.750
-0.748
ln(⁶²Ni/⁶⁰Ni)
-1.914
-1.916
-1.918
-1.920
-1.922
-1.924
-1.926
m = 0.994
r² = 0.998

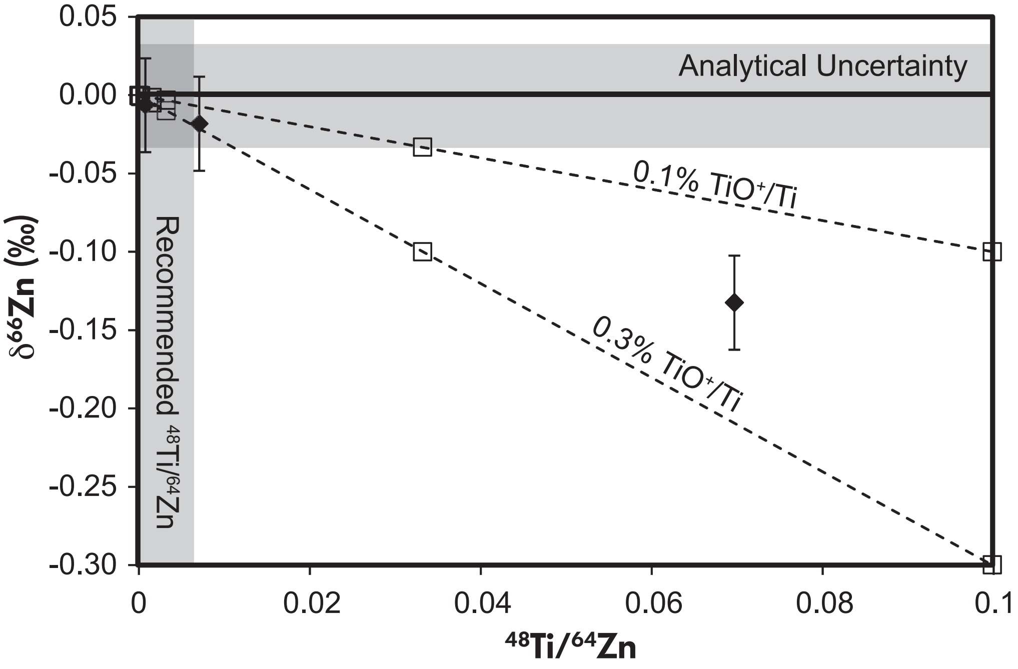
Analytical Uncertainty
0.1% TiO⁺/Ti
0.3% TiO⁺/Ti
Recommended ⁴⁸Ti/⁶⁴Zn
δ⁶⁶Zn (‰)
0.05
0.00
-0.05
-0.10
-0.15
-0.20
-0.25
-0.30
0
0.02
0.04
0.06
0.08
0.1
⁴⁸Ti/⁶⁴Zn